UNIVERSITY OF CINCINNATI

May 13, 19 98

I, Misoon Y. Mah,
hereby submit this as part of the requirements for the degree of:

Doctor of Philosophy

in Dept. of Electrical/Comp Eng. & Comp Science

It is entitled FDTD Simulation for Dimensional Analysis in Microwave Design

Approved by:

FDTD Simulation for Dimensional Analysis in Microwave Design

A dissertation submitted to the

Division of Research and Advanced Studies
of the University of Cincinnati

in partial fulfillment of the
requirements for the degree of

DOCTORATE OF PHILOSOPHY (Ph.D.)

in the Department of Electrical and Computer
Engineering and Computer Science
1998

by

Misoon Y. Mah

B.S., Sogang Jesuit University, 1969
M.S., University of Utah, 1972
B.S., University of Dayton, 1983

Committee Chair: Professor Altan M. Ferendeci

ABSTRACT

In this thesis, with the 3D MMIC elements development in mind, two rigorous design approaches have been attempted. First, dimensional analysis, a non-conventional methodology has been performed in scaled single microstrip lines to obtain the mathematical design expressions as a function of dimensionless products, π-terms. The design expressions have been driven for characteristic impedance and effective dielectric constant for the low and high frequency approximations. The analysis of mechanism for conductor and dielectric loss have been also discussed. However, due to its inherent limited capability, the finite-difference time-domain (FDTD) have been looked into as a full wave field solver to enhance the design capability of innovative 3D MMIC elements. The FDTD has been used to perform time-domain simulations of pulse propagation in scaled coupled microstrip lines. In addition to the time-marching results, frequency-dependent characteristic impedance, effective dielectric constant and phase velocity have been calculated by Fourier transform of the time-domain results. Some results have been verified by comparison with measured data. Most importantly, based on the premise that scaling results can be predicted by the dimensional analysis, experimental measurements are carried out on a coupled lines with dimensions different than simulated ones. Using FDTD results, an unique approach for developing lumped element models have been also discussed.

ACKNOWLEDGMENT

The author of this thesis would like to thank all of those individuals who help to make this dissertation possible. She thanks specially to Dr. Altan M. Ferendeci, the dissertation advisor, whose direction and continued guidance was essential to the success of this research. She also thanks to Mr. Robert Kemerley and Mr. Alan Tewksbury of the Aerospace Components & Subsystems Technology Division of the Air Force Research Laboratory's Sensors Directorate, for their encouragement and the opportunity to pursue higher education through the Long-Term Full Time Training Program. The author is grateful for the continuous assistance and encouragement provided by Dr. Lee Liou and Dr. Robert Ewing throughout the course of research. She thanks her dissertation committee for their encouraging comments and feedback on her dissertation.

The author also wants to thank her late parents for their endless motivation and support. They taught her to finish always once started. She also thanks to her mother-in-law, Mrs. Junk Suk Mah for her continuous support and encouragement. Finally, with all of her heart, she would like to thank her husband, Dr. Tai-Il Mah and their two sons, Brian and Jonathan Mah for their continuous care and encouragement.

Table of Contents

List of Figures

CHAPTER 1. INTRODUCTION

Currently many applications demand more compact and efficient Multichip Assembly (MCA) in the microwave and millimeter wave areas. As they reach increasing functionality levels, thereby reducing the cost and the size of microwave and millimeter-wave integrated circuits, the conventional MMIC technology needs to be reengineered to meet these requirements. However the current technology is limited because it is a 2D, planar technology. To accomplish these greater objectives, innovative 3D interconnect and integration technology is required from the chip level to the interface of the MCA with the host system. The integration level, *I*, defined as the product of gain (G in dB) and bandwidth ($\Delta f/fo$) divided by the surface area (in mm^2), obeys the curve of $I \times f^{1/2} = 2$. Above 10 GHz (X-band), *I* is typically less than .6, but it has been shown that 3D MMIC technology can increase the integration level threefold [1]. This indicates that 3D technology can significantly contribute to reducing cost and the size of MMICs without sacrificing functionality.

There has already been considerable research and development[1,2] of the 3D MMIC technology. However, further investigation on circuit design, electro-thermal simulation, multilayer dielectric materials, process development, component development, and assembly and characterization are still required to mature the 3D MMIC technology. There are two major approaches that utilize the 3D MMIC technology. One uses thin multiple dielectric layers (2.5 - 50 um each) with vertical interconnects. This approach allows for many design options for interconnects. The low dielectric constant material allows for less loss in transmission lines while minimizing volume needed for signal interconnect. The second approach is to stack one circuit module over the other using vertical interconnects. This generally does not allow for as many design options as the former approach. However, both approaches complement each other.

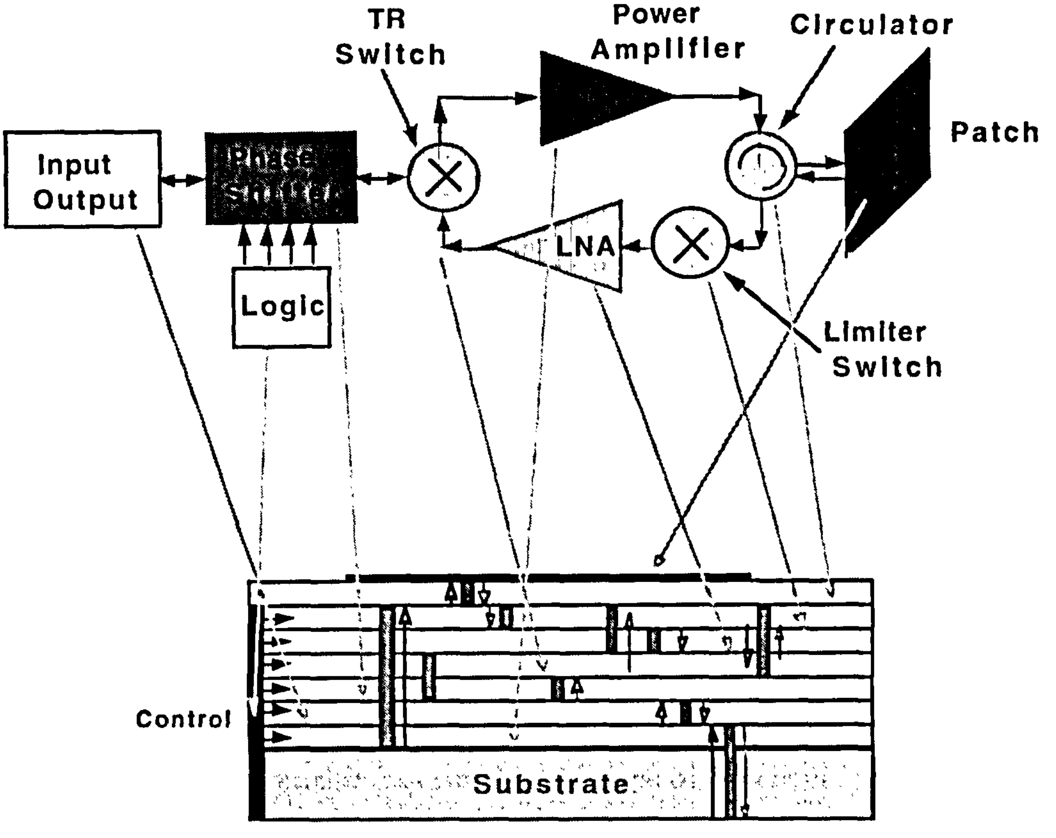

Figure 1.1 Major Part of 3D T/R Module

The development of 3D MMIC also opens up the possibility of a *conformal* technology. One of the main application areas is the modules of an electronically controlled phased array antenna system. In order for a module to be universally conformal to any arbitrarily curved surface, the depth of the module must be negligibly small compared to the maximum lateral dimension of the module. In comparison to this concept, current 2D technology has a distinct disadvantage because the depth of a typical module is too large compared to its lateral dimensions and can not be used in a conformal configuration.

As mentioned previously, to develop 3D MMICs, a new regime of 3D technology has to be investigated. Although the conventional 2D technology can be used as a stepping stone, 3D technology development will require substantial deviations from the existing technology in the area of circuit design, fabrication and characterization. For example, circuit simulation software such as Libra, MDS and Compact are available, however; they do not include the topology that will be used for the 3D MMICs. For example, the coplanar waveguide(CPW) model available in Libra includes only CPW surrounded with dielectric and air, but will not model the 3D CPW which is surrounded with homogeneous dielectric with upper and bottom ground planes. Since commercial software, such as Libra does not simulate this type of 3D circuit element, either a new 3D element has to be added to its library or an entirely innovative 3D library has to be developed in order to model the 3D MMIC elements accurately. The lack of capability to simulate 3D elements with the present library will cause substantial simulation errors, especially when resonant elements are used in a circuit.

Throughout the development of microwave design [3,4,5,6], designers have constantly confronted with complex problems. In order to take account the phenomena such as dispersion [7], loss and coupling parameters [8] into the design, designers have to know how to deal with discontinuities and inhomogeneous circuit environments that affect the design parameters. Particularly, the three dimensional (3D) microwave design requires more functional and compact design. As microwave circuits become more complex, the discontinuities and inhomogeneous environment have to be treated more accurately to provide reliable circuit parameters. . These discontinuities can no longer be treated as point sources even at the low frequencies. Especially, as the circuit elements become electrically long the network approach is no longer reliable in the microwave design [4].

In this thesis, with the 3D MMIC development in mind, two rigorous design approaches are attempted. The first approach is to implement dimensional analysis in the microwave circuit design area. The second approach is the Finite-Difference in Time Domain method to complement the dimensional analysis. The following will briefly describe each approach and how these will complement each other.

The first approach, dimensional analysis is a non-conventional methodology which is not relying on the algebraic (or numerical) solutions of the governing equations, which are Maxwell's wave equations. As will be explained in detail in Section II, dimensional analysis is implemented to establish the relationship between the circuit system parameters. This approach allows the designers to study the relationship between the system parameters, to identify independent system variables from dependent variables, redundant from irrelevant variables, and provides insight into the overviews of the circuit system. For example, in the microstrip design, typically, the ratio between the substrate thickness and the conductor width is taken into consideration to find the characteristic impedance of the microstrip line. It has always required this ratio rather than the width of the conductor or the substrate thickness alone. In most of the cases the designer takes it intuitively without putting much thoughts about why. This is allowed in the microwave design area because it has been conventionally executed in that manner in the past.

Dimensional analysis is a rigorous approach to find the relationship between the system parameters and allows to scale various parameters in a consistent manner using dimensionless product, π-terms. However dimensional analysis is limited to its inherent capability. Since it does not generate its own algebraic analytical solution of the governing equations, it is always required to be relied on other solutions to come up with its own mathematical design expressions. Therefore, dimensional analysis was performed in conjunction with the use of commercial circuit simulation tools, such as Microwave Harmonica and Explorer developed by Compact Software, Inc. A microstrip line is selected to obtain mathematical design expressions for characteristic impedance and effective dielectric constant for the low and high frequency approximations. The analysis of mechanisms for conductor and dielectric losses are also discussed [5].

To enhance the design capability of innovative 3D MMIC elements, the full wave field solver is required to simulate the denser discontinuities of the system. The FDTD method [15] is selected because the broad spectral information can be obtained from the full wave field solution computed by a single run of the FDTD. Since the field solution is calculated in the time-domain, a simple Fourier transformation of transient wave can easily generate microwave circuit parameters for the operating frequency of interest. The FDTD method also simulates time marching of electromagnetic wave over the computational domain as time stepping continues.

A coupled microstrip line is selected to verify the applicability of FDTD method to determine microwave parameters associated with microwave circuit elements. The choice is based on the premise that all parameters of coupled microstrip lines have been previously determined with various simulation methods as well as by experimental techniques. These parameters obtained from the FDTD method are for the first time compared to existing solutions [5,6] and verified by some experimental data.

Using the FDTD solution, an unique approach to develop an equivalent circuit of the coupled line is also discussed. Most importantly, based on the premise that scaling results [9] can be predicted by the dimensional analysis, experimental measurements are carried out on a coupled lines with dimensions different than simulated ones.

By complementing dimensional analysis and a full wave field solver, such as FDTD method, the rigorous design approach can be implemented to develop a more complicated circuits such as 3D MMIC circuit elements.

Following Introduction in Section I, Dimensional analysis and its applications will be discussed in Section II and III, respectively . In Section IV and V, Electromagnetic FDTD analysis and its application will be discussed. Finally, discussion and future research areas will be addressed in Section VI.

CHAPTER II. Dimensional Analysis

II.1 Background

Often designers ask themselves the following questions: What should they do first when they are just starting designing the system. Especially when the system is too complex for a complete theoretical treatment or a complete characterization. Such complexity might be resulted from a large number of variables (physical quantities) affecting the phenomenon, or from complicated mathematical equations expressed with these variables.

In designing such system, the designers should be allowed to simplify the system design by learning the relationships between these variables. By doing so they can identify independent variables of a system from dependent, redundant or irrelevant variables and gain the overviews of the system from the basic concept to more sophisticated ideas. This process allows the designer not only to reduce the number of variables, but also save time and cost by performing less experiments and simulations for the equal or better design of the system. This process can be possible using a methodology called dimensional analysis [10,11].

Dimensional analysis is a non-conventional methodology which is not relying on the algebraic analytical (or numerical) solutions of the governing equations. Generally it is implemented to establish the relationship between the system variables. A typical system involves a number of variables, and the relationship between these variables are usually not straightforward. In most cases, a specific performance of interest may not be affected by each individual variable alone, but by a certain relationship between these individual variables. Thus implementation of these relationships makes the design more efficient and the design cycle shortened.

Historically, the dimensional analysis has been introduced to the designers in numerous areas. The analysis has been applied to interpret the Rayligh scattering [10], in which the frequency dependency of the light scattering was established. The model of the skin depth phenomenon [10,11] of the ac conduction in the metal can also be derived using this analysis. In thermal dynamics, the relationship between pressure, volume and temperature in thermal equilibrium system was deduced with dimensional analysis. In solid mechanic system, the principle of dimensional analysis is applied to relate the data obtained using a scaled-down model to the performance prediction of the actual-size system. In fluid dynamics, the Reynolds number[3] is the dimensionless constant. The results of a single experiment of a model can be applied to a series of experiments using different models as long as the Reynolds number remains the same [11].

However, in the microwave design and characterization areas, dimensional analysis has not found such wide applications as in some other areas. This is because the microwave design is traditionally based on the solutions of the governing equations, namely the Maxwell's equations. Because of the complicated boundary conditions and inhomogeneity (discontinuity) in the microwave circuit, especially in MMICs (microwave monolithic integrated circuit) numerical approach is usually required to solve these equations. Microwave parameters, such as characteristic impedance, phase velocity and attenuation constants are also obtained from these solutions . The desired microwave parameters can be achieved by adjusting design variables such as the circuit geometry and the dielectric constants. The conventional microwave design methodology is based on the algebraic analysis of the mathematical equations, and has been adopted in the microwave design.

Currently, modeling precision reaching a fraction of a percent of accuracy can be achieved through the high cost and time of CAD (computer aided design and simulation). Therefore, accurate prediction of circuit performance through CAD is possible prior to fabrication and characterization, thus saves effort and time.

Implementing the dimensional analysis in conjunction with use of recent sophisticated electromagnetic simulations can save effort and time because it allows the designer to design the circuits more efficient and faster from the minimum number of simulations. However, to implement this analysis, the designer is required to have good knowledge in the electromagnetic area such that the designer should know which system variables need to be introduced to establish the relationship between the design variables, and which variables affect most the desired microwave phenomenon. With these knowledge one would enable to make a proper asymptotic approximation for the more efficient and faster design using dimensional analysis.

The dimensional analysis is briefly introduced in the following. The physical phenomenon can be described by certain relationships between the system variables. These variables may be expressed by analytical equation(s) or measured. They can also be represented by some quantities using a certain measuring units. Measuring units are usually a combination of the fundamental units of the irreducible dimensionally. In engineering and scientific regime, the MKS force system is commonly used and utilizes meter, kilogram, second and coulomb in measuring length, mass, time and charge, respectively.

In order for the dimensional analysis to be valid, the equation describing a certain physical phenomenon needs to be of dimensional completeness and dimensional homogeneity [10,11]. The equation is dimensionally complete if the functional relation of the equation remains unchanged when the fundamental unit of the measurement changes. The dimensional homogeneity is that any function of the dimensionless variable is dimensionless. This also means that as the relationship between variables are expressed mathematically, such as adding, subtracting or equating the dimensional formula of the variables has to be of same kind. With these two properties, it can be proved that the equation can be reduced to a relationship among a complete set of dimensionless products of the system variables. In the process, the exponents of a dimensionless product are obtained by a certain set of homogeneous linear algebraic equations. This is also known as the Pi(π)–theorem [10,11]. Apparently, since all the scientific and engineering equations posses these two properties, the dimensional analysis is applicable.

Section 2.1 describes Physical Algebra and p-Theorem, and the application of dimensional analysis to solving the microwave problems is shown in the subsequent sections. A microstrip transmission line is used as an example. It also shows derivations to calculate the characteristic impedance of the microstrip line as a function of w/h and ε_r at low frequencies, and as a function of w/h and hf at high frequencies using GaAs substrate, where w is the width of the transmission line, h is dielectric height, ε_r is the relative dielectric constant, and f is the frequency.

This work is performed in conjunction with the use of Microwave Harmonica and Explorer by Compact Software, Inc., EM by Sonnet Software, and HFSS and Microwave Lab by Ansoft. The explicit closed-form expressions of the microwave circuit parameters as functions of the design parameters are developed. The derived expressions can be applied in the practical circuit design. The similar analogy can be implemented to the experimental system to derive the closed-form expressions. In Section III.1.1 the circuit parameters of a lossless microstrip with low frequency approximation are extracted using dimensional analysis. The closed-form expressions are derived from curve fits using Kleidgraph and has agreed well with the analytical solution derived by I. Bahl [12].

In Section III.1.2, frequency dependent parameters of the microstrip line are extracted, and in Section III.2, conductor and dielectric loss are studied using dimensional analysis, and followed by results and discussion.

II.2 Physical Algebra and π-Theorem

The following sections describe the principle of the absolute significance of relative magnitude and general procedure of the dimensional analysis.

II.2.1 The principle of the absolute significance of relative magnitude

In physical systems, any measurable quantity will observe the principle of the absolute significance of relative magnitude. That is to say, the relative magnitude between the measurable quantities is independent of the particular magnitude chosen for each fundamental unit. This imposes the system variables are measured in terms of fundamental units. Suppose there are n fundamental units of irreducible dimensionality, u_1, u_2,....and u_n, and u_1', u_2',.... and u_n' measured in two different measurement systems, respectively. Introduce system variables, p and p' which are functions of $f(u_1, u_2,....,u_n)$ *and* $f(u_1', u_2',....., u_n')$, respectively. Now, the magnitude of the fundamental units, u_i and u_i' are changed by x_1, x_2,....and x_n. Using the principle of the absolute significance of relative magnitude :

$$\frac{p}{p'}=\frac{f(u_1,u_2,....,u_n)}{f(u_1',u_2',....,u_n')}=\frac{f(x_1u_1,x_2u_2,.....,x_nu_n)}{f(x_1u_1',x_2u_2',......,x_nu_n')} \qquad 2.1$$

This relationship holds for all values of u_1, u_2,....and u_n, u_1', u_2',....and u_n', and x_1, x_2,....and x_n. By rearranging the above expression:

$$f(x_1u_1,x_2u_2,.....,x_nu_n)=f(x_1u_1',x_2u_2',......,x_nu_n')\times\frac{f(u_1,u_2,....,u_n)}{f(u_1',u_2',....,u_n')} \qquad 2.2$$

Differentiate it partially with respect to x_1, and equate $x_1, x_2,....x_n=1$, then

$$u_1\frac{f_1(u_1,u_2,.....,u_n)}{f(u_1,u_2,....,u_n)}=u_1'\frac{f_1(u_1',u_2',....,u_n')}{f(u_1',u_2',....,u_n')}=....=\ u_1'''\frac{f_1(u_1''',u_2''',.....,u_n''')}{f(u_1''',u_2''',.....,u_n''')}=\frac{u_1}{f}\frac{\partial f}{\partial u_1}, \qquad 2.3$$

where $f_1=\dfrac{\partial f}{\partial u_1}$, and u_1 includes u_1, u_1',...,u_1'''. The expression is independent of u_1, therefore,

$$\frac{u_1}{f}\frac{\partial f}{\partial u_1}=C_1(u_2, u_3, \ldots\ldots, u_n), \text{ and } \frac{1}{f}\frac{\partial f}{\partial u_1}=\frac{C_1}{u_1} \qquad 2.4$$

which integrates to:

$$f=C_1 u_1^{const} \qquad 2.5$$

The above process is repeated, by differentiating partially successively with respect to x_2, x_3,..., and x_n, and integrating. Then, for the final expression, the function, f which represents the system variable, p becomes: $f = Cu_1^{b_1}u_2^{b_2}....u_n^{b_n}$, where b_1, b_2,...,b_n are constants. Therefore, any system variables which obey the principle of the absolute significance of relative magnitude are expressed with the product of an arbitrary constant and fundamental units with arbitrary exponents. This is true for all system variables which are measurable in scientific measurements.

II.2.2 General Procedures of the Dimensional Analysis

Suppose there are n fundamental units of irreducible dimensionality, u_1, u_2, ... and u_n, and the magnitude of each unit is arbitrarily set. A physical system involves m system variables, p_1, p_2, ... and p_m. These system variables are measurable according to the magnitude of each fundamental units and satisfy the requirement of the principle of the absolute significance of relative magnitude.

Thus, suppose there are system variables, $[p_i]$ which can be expressed by:

$$[p_i] = u_1^{b_{1i}} u_2^{b_{2i}} .....u_n^{b_{ni}}, \qquad 2.6$$

where b_{1i}, b_{2i}, ... and b_{ni} are the exponents,

and have a functional relation: $\phi(p_1, p_2, p_3, \ldots\ldots p_m)= 0$ 2.7

For the function, ϕ to be complete ϕ remains same regardless of the magnitude change in fundamental units. Then, introduce $[p_i] = u_1'^{b_{1i}} u_2'^{b_{2i}} .....u_n'^{b_{ni}}$ and $u_i' = x_i u_i$. u_i' is a fundamental unit meaured in a different measurement system and differ from u_i by the magnitude of x_i. Therefore,

$$p_1' = u_1'^{b_{11}} u_2'^{b_{21}} .....u_n'^{b_{n1}} = x_1^{b_{11}} u_1^{b_{11}} x_2^{b_{21}} u_2^{b_{21}} ....x_n^{b_{n1}} u_n^{b_{n1}} = (x_1^{b_{11}} x_2^{b_{21}} .....x_n^{n1}) p_1 \qquad 2.8$$

$$p_2' = u_1'^{b_{12}} u_2'^{b_{22}} .....u_n'^{b_{n2}} = x_1^{b_{12}} u_1^{b_{12}} x_2^{b_{22}} u_2^{b_{22}} ....x_n^{b_{n2}} u_n^{b_{n2}} = (x_1^{b_{12}} x_2^{b_{22}} .....x_n^{b_{n2}}) p_2 \qquad 2.9$$

$$p_m' = u_1'^{b_{1m}} u_2'^{b_{2m}} .....u_n'^{b_{nm}} = x_1^{b_{1m}} u_1^{b_{1m}} x_2^{b_{2m}} u_2^{b_{2m}} ....x_n^{b_{nm}} u_n^{b_{nm}} = (x_1^{b_{1m}} x_2^{b_{2m}} .....x_n^{b_{nm}}) p_m \qquad 2.10$$

Then, $\phi(p_1', p_2', p_3', ..., p_m')$

$$= \phi\{(x_1^{b_{11}} x_2^{b_{21}} .....x_n^{b_{n1}}) p_1, (x_1^{b_{12}} x_2^{b_{22}} .....x_n^{b_{n2}}) p_2, ...(x_1^{b_{1m}} x_2^{b_{2m}} .....x_n^{b_{nm}}) p_m\} = 0 \qquad 2.11$$

Note that if the expression, $\{f(x,p) - f(p)\}|_{x=1}=0$ is an identity, then the expression also holds for the differentiation of the function: $\{\frac{\partial\phi(x,p)}{\partial x} - \frac{\partial\phi(p)}{\partial x}\}_{x=1} = 0$

Differentiate partially with respect to x_1(using chain rule), and after the differentiation put all the x's equal to 1:

$$\frac{\partial\phi}{\partial x}|_{x=1} = \{\frac{\partial\phi}{\partial p'}\frac{\partial p'}{\partial x}\}|_{x=1} = 0$$

$$\text{Then, } b_{11}p_1\frac{\partial\phi}{\partial p_1} + b_{12}p_2\frac{\partial\phi}{\partial p_2} + ... + b_{1m}p_m\frac{\partial\phi}{\partial p_m} = 0 \qquad 2.12$$

Let $p_1'' = p_1^{\frac{1}{b_{11}}}, p_2'' = p_2^{\frac{1}{b_{12}}}, ..., p_m'' = p_m^{\frac{1}{b_{1m}}}$, then $\frac{\partial p_i''}{\partial p_i} = \frac{1}{b_{1i}} p_i^{\frac{1}{b_{1i}}-1}$, and

$$\frac{\partial\phi(p_i'')}{\partial p_i} = \frac{\partial\phi}{\partial p_i''}\frac{\partial p_i''}{\partial p_i} = \frac{\partial\phi}{\partial p_i''}\frac{1}{b_{1i}} p_i^{\frac{1}{b_{1i}}-1}$$

Substitute this into the equation 2.12

$$\text{then, } p_1''\frac{\partial\phi}{\partial p_1''} + p_2''\frac{\partial\phi}{\partial p_2''} + ... + p_m''\frac{\partial\phi}{\partial p_m''} = 0 \qquad 2.13$$

With the equation 2.13 we can prove that $\phi(p_1'', p_2'', ...p_m'')$ is actually $\phi(z_1, z_2, ...z_{m-1})$,

where $z_1 = \frac{p_1''}{p_m''}, z_2 = \frac{p_2''}{p_m''}, ...z_{m-1} = \frac{p_{m-1}''}{p_m''}, z_m = 1$

To prove $\phi(p_1^{''}, p_2^{''}, \ldots\ldots p_m^{''}) = \phi(z_1 p_m^{''}, z_2 p_m^{''}, \ldots\ldots, z_{m-1} p_m^{''}, p_m^{''})$

$$\frac{\partial\phi}{\partial p_m^{''}} = \frac{\partial\phi}{\partial p_i^{''}}\frac{\partial p_i}{\partial p_m^{''}} = z_1\frac{\partial\phi}{\partial p_1^{''}} + z_2\frac{\partial\phi}{\partial p_2^{''}} + \ldots\ldots + z_{m-1}\frac{\partial\phi}{\partial p_m^{''}} + \frac{\partial\phi}{\partial p_m^{''}}$$

$$= (p_1^{''}\frac{\partial\phi}{\partial p_1^{''}} + p_2^{''}\frac{\partial\phi}{\partial p_2^{''}} + \ldots\ldots + p_m^{''}\frac{\partial\phi}{\partial p_m^{''}}) / p_m^{''}$$

$$= 0 \qquad 2.14$$

This indicates that the function f is independent of $p_i^{''}$.

Then, we may write

$$\phi(p_1^{''}, p_2^{''}, \ldots\ldots p_m^{''}) = \phi(z_1 p_m^{''}, z_2 p_m^{''}, \ldots\ldots, z_{m-1} p_m^{''}, p_m^{''}) = \varphi_1(z_1, z_2, \ldots\ldots, z_{m-1}) = 0, \qquad 2.15$$

where φ_1 is a function of m-1 arguments rather than m. Note that since all the quantities $p_i^{''}$ are constructed with the first degree in the first fundamental unit, u_1, the ratio, z_i's are dimensionless in u_1, i.e. u_1^0.

Now the number of argument may be reduced further by setting $\varphi_1(z_1, z_2, \ldots\ldots, z_{m-1}) = 0$. φ_1 has been proved to be identical as ϕ, but with m-1 arguments. By differentiating φ_1 with respect to x_2, the procedure above from the equation (1) is repeated to reduce the number of arguments by one more. Then, the function, $\varphi_2(z_1, z_2, \ldots\ldots, z_{m-2})$ becomes dimensionless in u_2. This procedure is repeated until all the fundamental units become dimensionless. The final function becomes a function of m-n arguments: $\varphi_n(z_1, z_2, \ldots\ldots, z_{m-n}) = \Phi(\pi_1, \pi_2, \ldots\ldots, \pi_{m-n}) = 0$, where π's are the m-n independent products of the system parameters, p_1, p_2,......, p_m and dimensionless in the fundamental units. This is known as the Π theorem and has been first explicitly driven by Buckingham in 1914. Due to the principle of dimensional homogeneity each dimensionless product, π term can be expressed by : $\pi_1 = \Psi(\pi_2, \pi_3, \ldots\ldots, \pi_{m-n})$ and consequently,

$$p_1^{a_1} = (p_2^{-a_2} \ldots\ldots p_m^{-a_m})\Psi(\pi_2, \pi_3, \ldots\ldots, \pi_{m-n}), \qquad 2.17$$

where $\pi = p_1^{a_1} p_2^{a_2} ......p_m^{a_m}$ and a_1, a_2, ... and a_m are the exponents. The unit of π is given by:

$$[\pi] = u_1^{\Sigma a_i b_{1i}} u_2^{\Sigma a_i b_{2i}} ....u_n^{\Sigma a_i b_{ni}} \qquad 2.18$$

where the summation index i in the exponent is running from 1 to m. Since π is dimensionless, a system of equations can be set up to solve for a_1, a_2, ... and a_m:

$$\begin{bmatrix} b_{11} & b_{12} & . & . & b_{1m} \\ b_{21} & b_{22} & . & . & b_{2m} \\ . & . & . & . & . \\ . & . & . & . & . \\ b_{n1} & b_{n2} & . & . & b_{nm} \end{bmatrix} \bullet \begin{bmatrix} a_1 \\ a_2 \\ . \\ . \\ a_m \end{bmatrix} = \begin{bmatrix} 0 \\ 0 \\ 0 \\ 0 \\ 0 \end{bmatrix} \qquad 2.19$$

This system of equations yields only a finite number of non-trivial independent solutions. The finite number of independent solutions, according to matrix algebra, is equal to the number of system variable minus the rank of the matrix B [11,13]. Each independent solution results in a dimensionless π term. After all the π terms are determined, the dependency between the system parameters can be established according to Pi theorem.

CHAPTER III. Application of Dimensional Analysis of Microstrip Line

III.1 Dimensional Analysis of Microstrip Line in Lossless System

Dimensional analysis has been implemented to a single microstrip lines to obtain the mathematical expressions as a function of dimensionless product, π-terms for the low frequency approximation and the frequency dependency.

III.1.1 Low Frequency Approximation:

Figure 3.1 shows a cross section of a microstrip line. The substrate thickness is h_1, the thickness above the substrate is h_2, the microstrip line width is w and the lateral dimension is L. The dielectric constants in and above the substrate are ε_1 and ε_2, respectively. The bottom and the top horizontal surfaces of the domain are assuming electrical walls, and the two vertical surfaces are assuming magnetic walls. Under the approximation of the quasi-TEM, the characteristic impedance Z_c [13,14,31] is defined to be the static voltage between the microstrip line and the ground plane divided by the static current in the microstrip line. These quantities are the static solutions to the Maxwell's equations, and they can be simulated and measured.

At low frequencies, wave propagation in the microstrip line can be approximated as quasi-TEM mode. Z_c approaches an asymptotic value as frequency, f becomes small.

In applying the dimensional analysis, the system variables and their corresponding units need to be determined. The system variables are h_1, h_2, w, L, ε_1, ε_2, and Z_c. The corresponding units of ε_1 , for example, be represented as Farad/meter=$[M]^{-1}[L]^{-3}[T]^2[Q]^2$, where [M], [L], [T], and [Q] stand for the fundamental units of mass, length, time and electrical charge, respectively. The exponents of each unit, -1, -3, 2 and 2 form the colum vector of the following matrix [B]. A dimensional constant of c, the speed of light in a vacuum is also called for in the analysis. Therefore, the matrix [B] is derived in the following accroding to the Pi theorem.

$$\begin{array}{c|cccccccc} & h_1 & h_2 & w & L & \varepsilon_1 & \varepsilon_2 & c & Z_c \\ \hline [M] & 0 & 0 & 0 & 0 & -1 & -1 & 0 & 1 \\ [L] & 1 & 1 & 1 & 1 & -3 & -3 & 1 & 2 \\ [T] & 0 & 0 & 0 & 0 & 2 & 2 & -1 & -1 \\ [Q] & 0 & 0 & 0 & 0 & 2 & 2 & 0 & -2 \end{array} \qquad 3.1$$

The rank of this matrix is 3. The number of the π terms is therefore, 8-3=5. The five independent solutions of [A] resulted in the following π terms:

$$\pi_1 = h_2/h_1,\ \pi_2=w/h_1,\ \pi_3=L/h_1,\ \pi_4=\varepsilon_1/\varepsilon_2,\ \pi_5=c\varepsilon_2 Z_c \qquad 3.2$$

According to the Pi theorem, the characteristic impedance, Z_c becomes a dependent function, ϕ of the π terms:

$$Z_c = \frac{1}{c\varepsilon_2}\phi\left(\frac{h_2}{h_1}, \frac{w}{h_1}, \frac{L}{h_1}, \frac{\varepsilon_1}{\varepsilon_2}\right) \qquad 3.3$$

III.1.2 Frequency Dependence

As frequency increases, quasi-TEM approximation becomes less applicable, and the dispersive nature becomes increasingly enhanced. In the microwave circuit, the characteristic impedance Z_c of the dominant mode is no longer unique for the higher modes. To study the dispersion of Z_c at higher frequencies, the frequency, f needs to be added into the set of the system variables. Applying the same procedures as before, one obtains the matrix[B] given by:

$$
\begin{array}{c|ccccccccc}
 & h_1 & h_2 & w & L & \varepsilon_1 & \varepsilon_2 & c & f & Z_c \\
\hline
[M] & 0 & 0 & 0 & 0 & -1 & -1 & 0 & 0 & 1 \\
[L] & 1 & 1 & 1 & 1 & -3 & -3 & 1 & 0 & 2 \\
[T] & 0 & 0 & 0 & 0 & 2 & 2 & -1 & -1 & -1 \\
[Q] & 0 & 0 & 0 & 0 & 2 & 2 & 0 & 0 & -2
\end{array}
\qquad 3.4
$$

The rank of this matrix is again 3. The number of the π terms is therefore, 6 and they are:

$$\pi_1 = h_2/h_1,\ \pi_2 = w/h_1,\ \pi_3 = L/h_1,\ \pi_4 = \varepsilon_1/\varepsilon_2,\ \pi_5 = fh_1/c,\ \pi_6 = c\varepsilon_2 Z_c \qquad 3.5$$

The characteristic impedance, Z_c from the Pi theorem becomes,

$$Z_c = \frac{1}{c\varepsilon_2}\phi\left(\frac{h_2}{h_1},\frac{w}{h_1},\frac{L}{h_1},\frac{\varepsilon_1}{\varepsilon_2},\frac{fh_1}{c}\right) \qquad 3.6$$

A further simplification of the dependencies of Z_c on the design parameters will be followed.

III.1.3 Results and Discussion

In the practical consideration for the microstrip line design, one may further simplify the functional dependence for Z_c, $Z_c = \phi(\frac{w}{h},\varepsilon_r,hf)$ in Section II.B. The calculated results of the characteristic impedance as a function of w/h with relative dielectric constant, ε_r are shown in Fig. 2. The data of Figure 3.2 was obtained from the simulated results using Microwave Harmonica developed by Super-Compact. Using least square fitting to the third order of $log(w/h)$ and ε_r, Z_c at low hf can be expressed by:

$$Z_c = m_0(\varepsilon_r) + m_1(\varepsilon_r)\log(w/h) + m_2(\varepsilon_r)(\log(w/h))^2 + m_3(\varepsilon_r)(\log(w/h))^3$$

$$
\begin{aligned}
m_0(\varepsilon_r) &= 126.27 - 101.79\log(\varepsilon_r) + 24.25(\log(\varepsilon_r))^2 \\
m_1(\varepsilon_r) &= -129.67 + 91.32\log(\varepsilon_r) - 16.06(\log(\varepsilon_r))^2 \\
m_2(\varepsilon_r) &= 20.82 - 1.88\varepsilon_r + 0.13\varepsilon_r^2 - 0.0043\varepsilon_r^3 \\
m_3(\varepsilon_r) &= 16.48 - 3.55\varepsilon_r + 0.35\varepsilon_r^2 - 0.011\varepsilon_r^3
\end{aligned}
\qquad 3.7
$$

The correlation between m_0 and m_1 with ε_r is more than 99.9% while the correlation between m_2 and m_3 with ε_r are 97 and 94%, respectively. Therefore, the accuracy of this fitting is more than 99% for the lower range of the values of w/h and ε_r. However, for the values of *w/h* close to 10 and ε_r close to 12 the accuracy falls to 93%.

Zc s were computed using above equation for $\varepsilon_1 = 10, \frac{w}{h_1} = .1, 1, 10$ and compared to the results obtained using the analytical solution[8, 11] derived by I.Bahl [12].

$e_1 = 10$	*Zc* from dimensional analysis	*Zc* from I.Bahl
w/h =0.1	108.24 ohms	106.84 ohms
w/h =1	48.73 ohms	48.73 ohms
w/h =10	9.88 ohms	8.35 ohms

For the lossless microstrip analysis the algebraic solutions are readily available because numerous work have been done. The above comparison is very reasonable.

With this formula, the other important design parameter of effective dielectric constant ,ε_{eff} can be calculated by $\varepsilon_{eff} = (Z_c^0/Z_c)^2$, where Z_c^0 is the characteristic impedance when $\varepsilon_r=1$

At certain occasions, the inverse function of the previous formula for Z_c is desirable; that is to find a *w/h* value for a desired characteristic impedance Z_c. The inverse formula is given in the following:

$$\log(w/h)=m_0 + m_1(\varepsilon_r)\log(Z_c) + m_2(\varepsilon_r)\{\log(Z_c)\}^2 + m_3(\varepsilon_r)\{\log(Z_c)\}^3 \qquad 3.8$$

$$m_0(\varepsilon_r)= 11.567 - 2.1389\varepsilon_r + 0.22275\varepsilon_r^2 - 0.0078438\varepsilon_r^3$$

$m_1(\varepsilon_r)= -16.04 + 2.6919\varepsilon_r - 0.27687\varepsilon_r^2 + 0.0097126\varepsilon_r^3$

$m_2(\varepsilon_r)= 8.492 - 1.0939\varepsilon_r + 0.11193\varepsilon_r^2 - 0.0039254\varepsilon_r^3$

$m_3(\varepsilon_r)= -1.6246 + 0.10897\varepsilon_r - 0.012291\varepsilon_r^2 + 0.00044204\varepsilon_r^3$

The accuracy of above relation for w/h is more than 90% for the range of w/h=0.1 through 10.

The dependency of $h_f f$ with w/h=0.25, 0.5, 1.0 and 2.0 and ε_r = 12.9 is shown in Figure 3.3. Z_c as a function of hf and w/h with a GaAs substrate (ε_r = 12.9) is given in the following using the least square fitting technique

$$Z_c\,(w/h,\ hf)= \gamma(hf)Z_c(w/h) \qquad 3.9$$

$$\gamma(hf) = 1.000 - 0.0017944(hf) + 0.00057115(hf)^2 \qquad 3.10$$

where $Z_c(w/h)$ is a characteristic impedance at low frequencies and γ is a correction factor due to the dispersion. The accuracy of the fitting is more than 95%.

III.2 Dimensional Analysis of Microstrip Line in Lossy System

Power loss is an important parameter in the microwave circuit design. In this section, we discuss the power loss due to microstrip conductor and the substrate dielectric material. The loss factor, $\alpha = \alpha_c + \alpha_\varepsilon$, where α_c and α_ε are the conductor and dielectric losses, respectively.

III.2.1 Conductor Loss

The metal resistivity and thickness, ρ and t, are included in the set of the system parameters. The matrix[B] is:

$$\begin{array}{c|cccccccccc} & h_1 & h_2 & w & L & \varepsilon_1 & \varepsilon_2 & f & t & \rho & \alpha_c \\ [M] & 0 & 0 & 0 & 0 & -1 & -1 & 0 & 0 & 1 & 0 \\ [L] & 1 & 1 & 1 & 1 & -3 & -3 & 0 & 1 & 3 & -1 \\ [T] & 0 & 0 & 0 & 0 & 2 & 2 & -1 & 0 & -1 & 0 \\ [Q] & 0 & 0 & 0 & 0 & 2 & 2 & 0 & 0 & -2 & 0 \end{array} \qquad 3.11$$

The rank of this matrix is 3. The number of the π term is 7. Again, some of the π terms are trivial, and are similar to those obtained previously. The set of π terms are:

$$\pi_1 = h_2/h_1,\ \pi_2=w/h_1,\ \pi_3=L/h_1,\ \pi_4=t/h_1,\ \pi_5=\varepsilon_1/\varepsilon_2,\ \pi_6=\varepsilon_2\rho t,\ \pi_5=h_1\rho \qquad 3.12$$

Therefore, from π_7, one obtains the functional relation for α_c:

$$\alpha_c = h_1^{-1}\phi(\frac{h_2}{h_1},\frac{w}{h_1},\frac{L}{h_1},\frac{t}{h_1},\frac{\varepsilon_1}{\varepsilon_2},\varepsilon_2\rho f) \qquad 3.13$$

A further simplification will be discussed.

III.2.2 Dielectric Loss

In this case, the real and imaginary parts of the dielectric constants of the substrate are considered. The system parameters and matrix[B] are in the following:

$$\begin{array}{c|cccccccccc} & h_1 & h_2 & w & L & \varepsilon_r & \varepsilon_r\tan\delta_\varepsilon & \varepsilon_2 & f & c & \alpha_\varepsilon \\ [M] & 0 & 0 & 0 & 0 & -1 & -1 & -1 & 0 & 0 & 0 \\ [L] & 1 & 1 & 1 & 1 & -3 & -3 & -3 & 0 & 1 & -1 \\ [T] & 0 & 0 & 0 & 0 & 2 & 2 & 2 & -1 & -1 & 0 \\ [Q] & 0 & 0 & 0 & 0 & 2 & 2 & 2 & 0 & 0 & 0 \end{array} \qquad 3.14$$

where $\varepsilon_r\tan\delta_\varepsilon$ is the parameter utilizing the commonly used material parameter of loss tangent, $\tan\delta_\varepsilon$. The rank of this matrix is 3. The number of the π terms is 7. Again, some of the π terms are trivial, and are similar to those obtained previously. The set of π terms are:

$\pi_1 = h_2/h_1,\ \pi_2 = w/h_1,\ \pi_3 = L/h_1,\ \pi_4 = \varepsilon_1/\varepsilon_2,\ \pi_5 = \tan\delta_1,\ \pi_6 = h_1 f/c,\ \pi_7 = h_1\alpha_\varepsilon$ 3.15

Therefore, from π_7, one obtains the functional relation for α_ε:

$$\alpha_\varepsilon = h_1^{-1}\phi(\frac{h_2}{h_1},\frac{w}{h_1},\frac{L}{h_1},\frac{\varepsilon_r}{\varepsilon_2},\frac{h_1 f}{c},\tan\delta_\varepsilon) \quad 3.16$$

III.2.3 Results and Discussion

The arguments of h_2/h_1 and L/h_1 in the dependency formula for α_c can also be omitted due to the same reason described above. The power attenuation due to the conducctor loss is therefore, simplified as:

$$\alpha_c = h^{-1}\phi(\frac{w}{h},\frac{t}{h},\varepsilon_r,\rho f) \quad 3.17$$

Again, ε_2 is assumed to be 1, and ε_r and h are the relative dielectric constant and the thickness of the substrate. The α_c as a function of the parameters,*w/h* with *t/h* is shown in Figure 3.4, while the α_c as a function of the parameters, ρf with *t/h* and w/h is shown in Figure 3.5. One notes that as the thickness of metal, and *w/h* increase, conductor loss decreases. As ρf increases, conductor loss also increases. The numerical results shows a square root dependence of ρf. This is due to the skin depth effect.

Based on the same assumption, the power attenuation due to the dielectric loss is simplified as:

$$\alpha_\varepsilon = h^{-1}\phi(\frac{w}{h},\varepsilon_r,hf,\tan\delta_\varepsilon) \quad 3.18$$

The dielectric loss α_ε as a function of *w/h* with *hf* and $\tan\delta_\varepsilon$ is shown in Figure 3.6. The figure shows that dielectric loss increases as *w/h* increases. The loss increases sharply, where *w/h*<2, but slows down with linear increase. The dielectric loss α_ε as a function of $\tan\delta_\varepsilon$ with parameters, *hf* and *w/h* is shown in Figure 3.7. Dielectric loss increases as loss tangent($\tan\delta_\varepsilon$) and hf increase. The numerical results show that the dielectric loss is proportional to both the loss tangent and frequency.

Dimensional analysis was applied to develop a new design methodology in the microwave integrated circuit design area. This work is a first known application of dimensional analysis in the microwave integrated circuit design. This novel approach towards microwave design provides the insight for developing scalable microwave performance models. The results show a complete dependency of the dimensionless product terms for the microwave parameters of the characteristic impedance, effective dielectric constant and the operating frequency, and leads to a scalable microstrip line model. This approach will benefit the microwave integrated circuit design area as a performance bound design methodology.

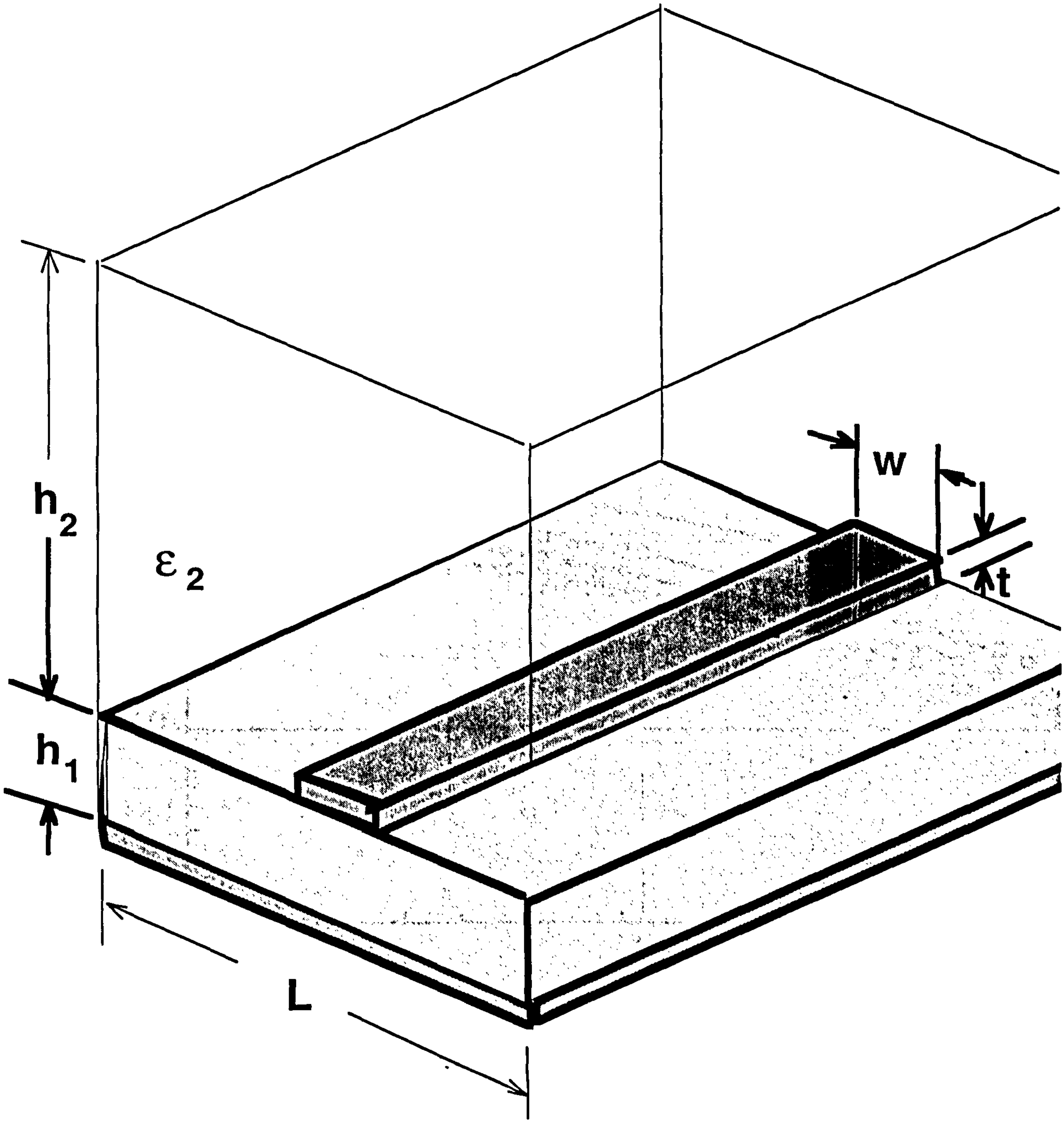

Figure 3.1 Microstrip Line

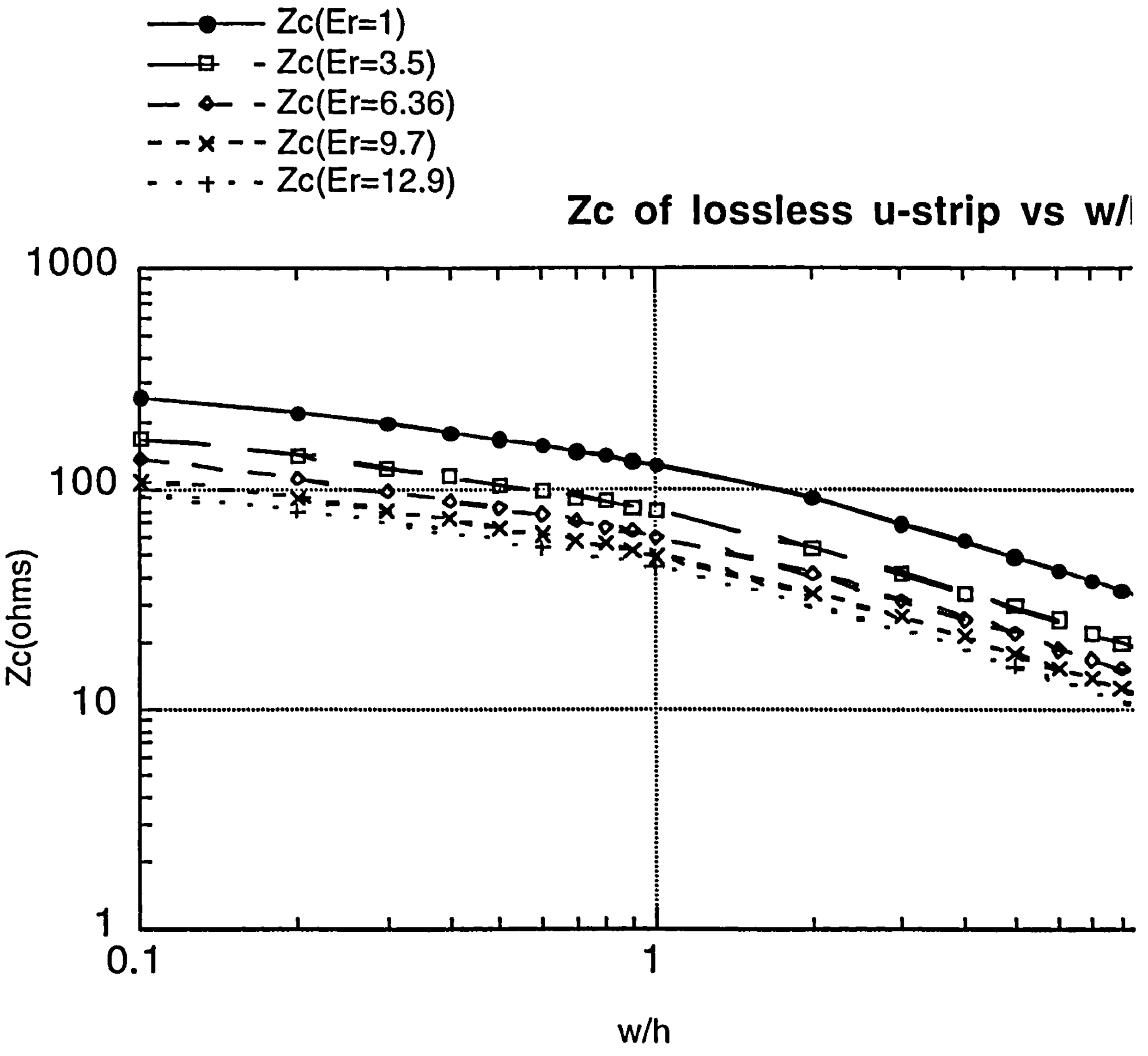

Figure 3.2 *Zc* as functions of *w/h* and ε_r

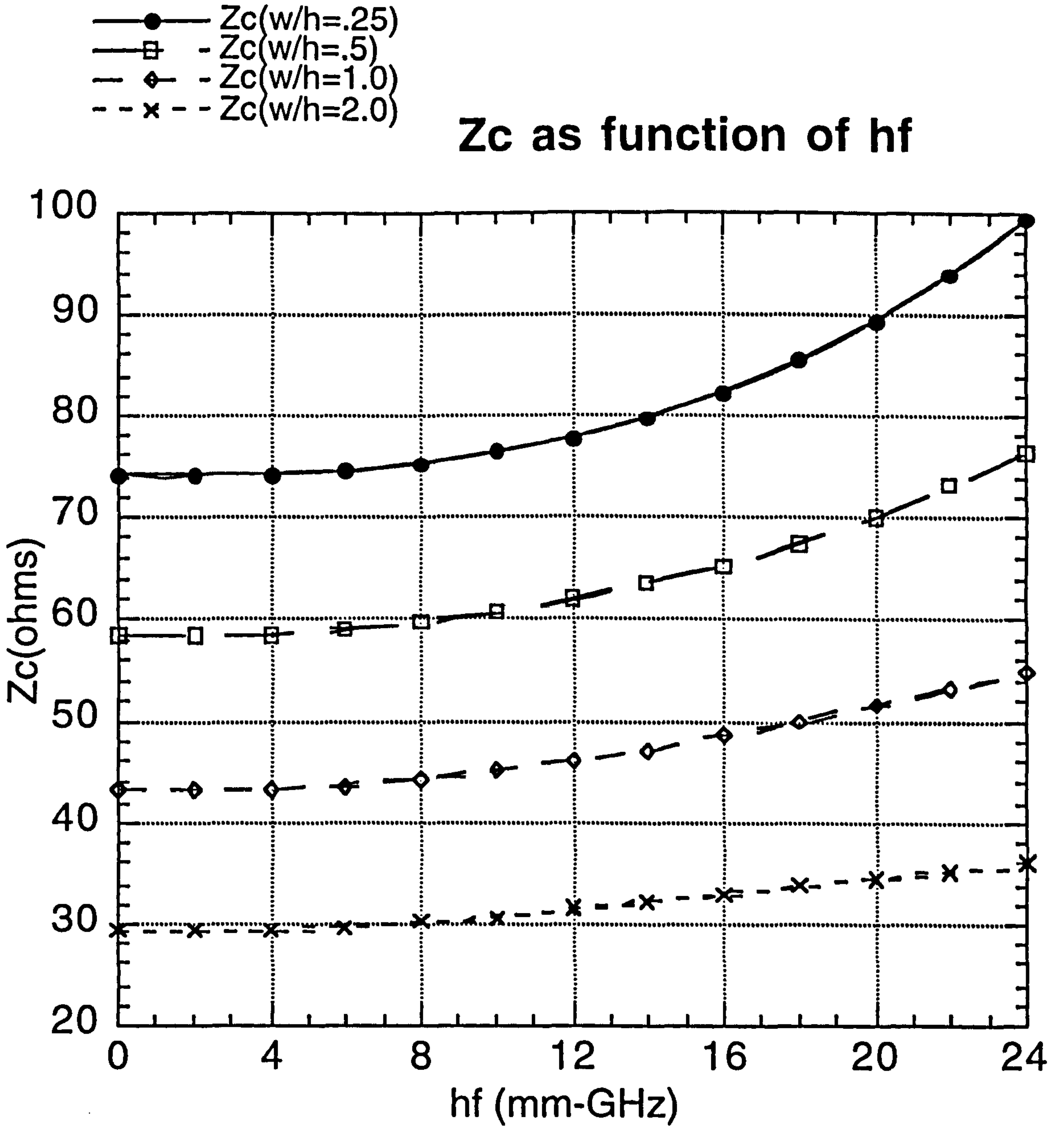

Figure 3.3 Characteristic Impednce (*Zc*) as function of *w/h* and *hf*

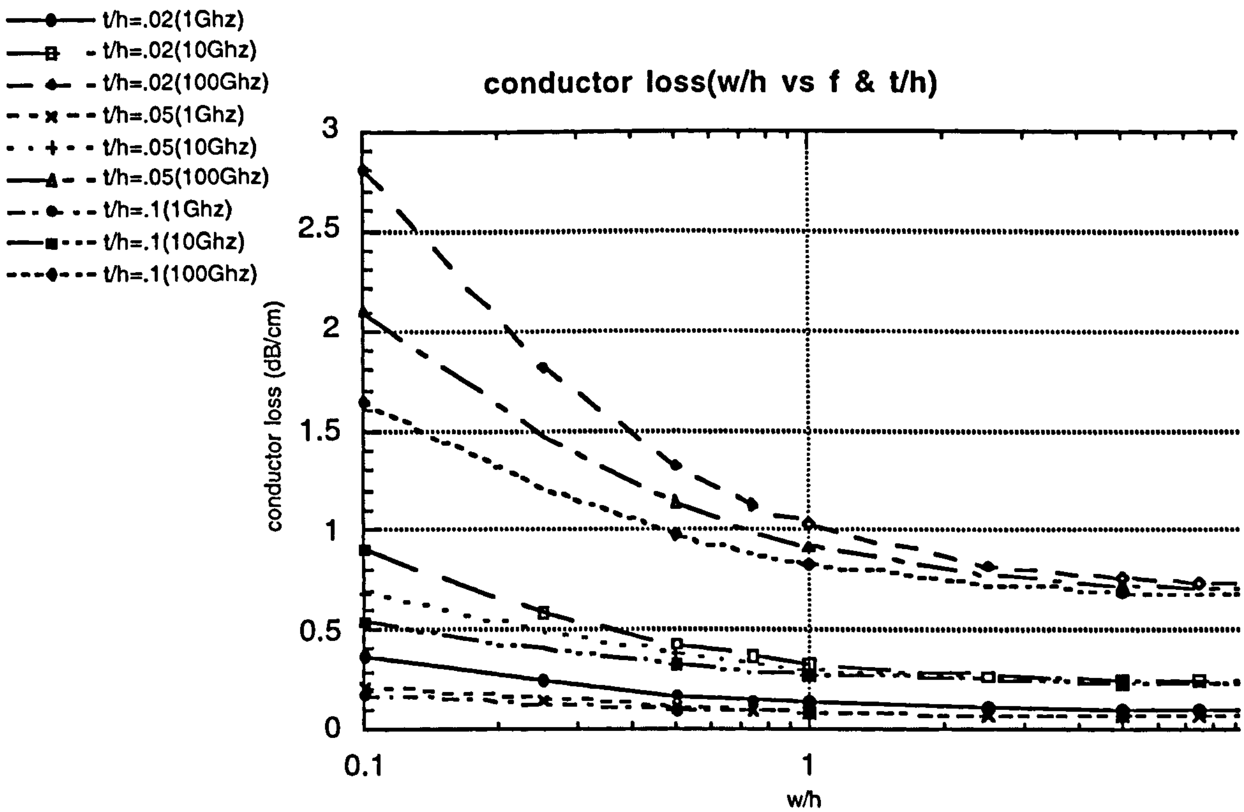

Figure 3.4 Conductor Loss as function of *w/h*, frequency and *t/h*

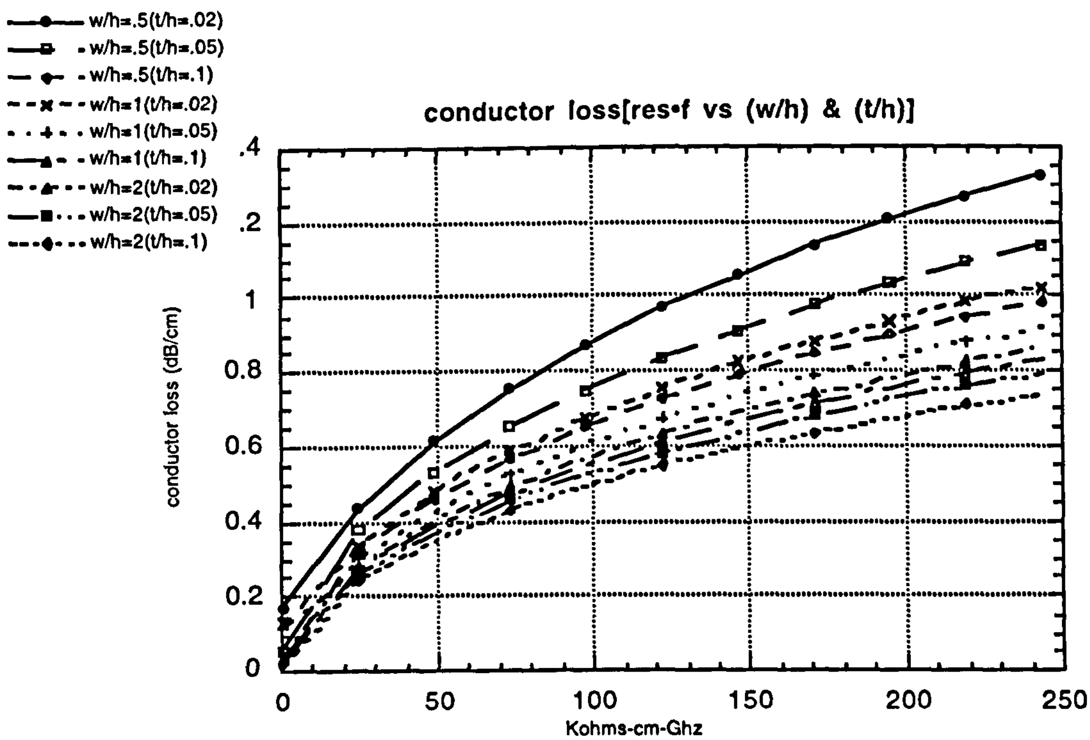

Figure 3.5 Conductor Loss as function of normalized frequency with *w/h* and *t/h*

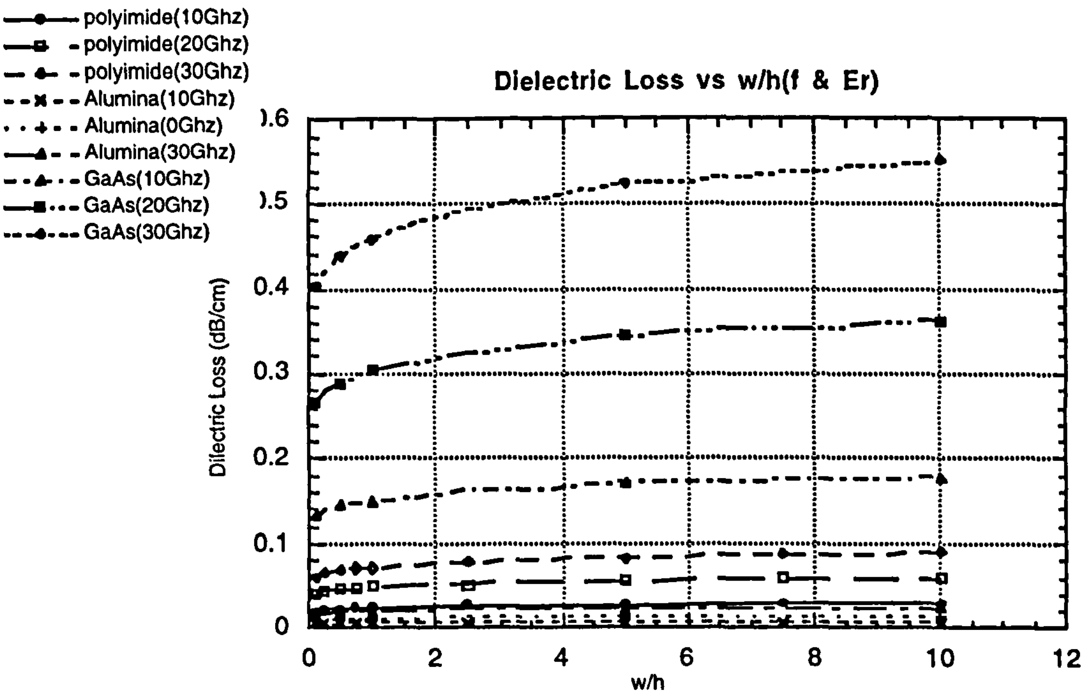

Figure 3.6 Dielectric Loss as function of *w/h* with frequency and ε_r

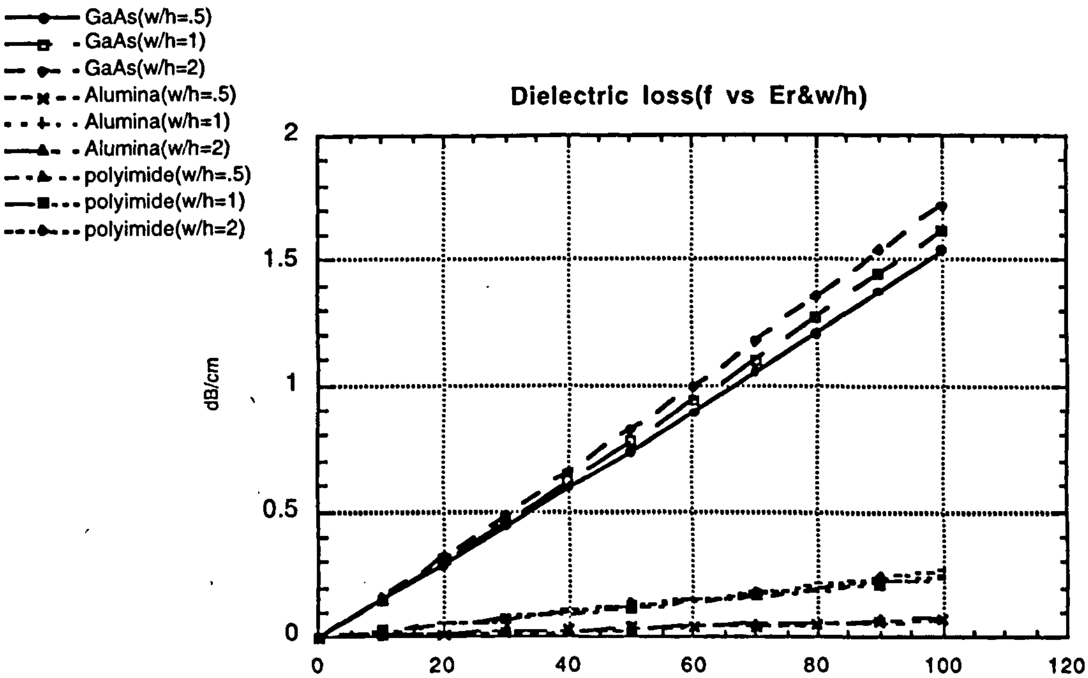

Figure 3.7 Dielectric Loss as function of frequency with w/h and ε_r

CAHAPTER IV. Electromagnetic FDTD Analysis

IV.1 Background

A direct three-dimensional finite-difference time-domain (FDTD) method is applied to the full-wave analysis of various coupled microstrip lines. The FDTD method allows to solve partial differential Maxwell's equation avoiding limitations of existing linear algebra technology which constrains the size of matrix required for solving integral form in such as frequency domain finite-element methods (FEM) or as in the methods of moments (MOM) [15]. It also allows to solve Maxwell's time dependent curl equations without introducing vector and scalar potentials. With appropriate boundary conditions and stability considerations, unknown electric field ($\vec{E}$) and magnetic fields ($\vec{H}$)are computed over computational domain. The boundary condition is chosen such that the reflected wave from the boundary should be negligibly small to be allowed in the vicinity of the structure of interest. In this study, Mur's second order absorbing boundary condition [15,16] is used. For the stability concern, the time step is derived based on spacial increments setting an eigenvalue problem. The space increment is chosen to prevent from the spurious results.

The key feature of the FDTD analysis is that the broad spectral information can be obtained from the full wave field solution computed by a single run of the FDTD [17]. Since the field solution is calculated in the time-domain, a simple Fourier transformation of transient wave can easily generate microwave circuit parameters of interest. The FDTD method also simulates time marching of electromagnetic wave over the computational domain as time stepping continues. The time marching results are shown in the result section.

The following sections describe how to formulate the FDTD method utilizing Maxwell's two curl equations. They also show how Yee's algorithm is implemented to predict accurate numerical results by avoiding numerical dispersion.

From the time-domain results, the frequency-dependent scattering parameters, odd(Z_{0o})-even(Z_{0e}) impedances, effective dielectric constants (ε_{eff}), and coupling coefficients are computed . The lumped equivalent circuit model is also discussed from the FDTD results. The circuits are fabricated , characterized and compared to the results obtained from the FDTD analysis, and shown in good agreement with numerically obtained scattering paramerters.

IV.2 FDTD Formulation

Maxwell's curl equations are discretized for the formation of the FDTD method over a finite volume using Yee's algorithm [18] called "leapfrog" method. The partial derivatives are approximated with centered difference approximations(mean value theorem, Euler's forward or backward method). Conducting surfaces are treated with Perfect Electric Conductor(PEC) so the tangential electric field components become zero. All the surrounding surfaces except the ground plane are treated with the second order Mur's absorbing boundary conditions(ABC) to prevent any unwanted reflection from surroundings.

IV.2.1 Governing Equations

The differential form of Maxwell's two curl equations are considered to be formulated with the FDTD method for a given system. The system to be analyzed is assumed to have no electric or magnetic current sources but has dielectric material which is influenced by the electric and magnetic energy. The Maxwell's equations govern the propagation of electromagnetic field in the system. In this work, the propagation media is assumed homogeneous, isotropic and uniform so that the piecewise approximation can be implemented. The system is also assumed to have no conductor and dielectric loss. With these assumptions, Maxwell's curl equations may simply is written as [15]:

$$\mu \frac{\partial \vec{H}}{\partial t} = -\nabla \times \vec{E} \qquad 4.1$$

$$\varepsilon \frac{\partial \vec{E}}{\partial t} = \nabla \times \vec{H} \qquad 4.2$$

Based on the assumption of the lossless structure, the approximate solutions to the differential equations are obtained by discretizing space and time over a finite three dimensional computational time domain with absorbing boundary conditions forced on surrounding walls.

IV.2.2 Finite-Difference Method

Finite difference method has been considered as the most popular numerical method to solve differential equations. Approximated values are obtained for the solution at a set of grid points x_i, where $i = 0, 1, \ldots..$ and the value at each x_i is obtained from some of the values computed in the previous steps.

Suppose a function, $u(x)$ and its derivatives are single valued, finite and continuous function of x, then Taylor's forward and backward series expansion of $u(x, t)$ can be implemented about the space point x_i to the space points $x_i + \Delta x$ and $x_i - \Delta x$,keeping time fixed at t_n :

using forward difference Taylor's series expansion [19],

$$u(x_i+\Delta x)|_{t_n} = u|_{x_i,t_n} + \Delta x \cdot \frac{\partial u}{\partial x}|_{x_i,t_n} + \frac{\Delta x^2}{2} \cdot \frac{\partial^2 u}{\partial x^2}|_{x_i,t_n} + \frac{\Delta x^3}{6} \cdot \frac{\partial^3 u}{\partial x^3}|_{x_i,t_n} + \frac{\Delta x^4}{24} \cdot \frac{\partial^4 u}{\partial x^4}|_{x_i,\xi_n} \qquad 4.3$$

$$x_i \le \xi \le x_{i+1}$$

The last term is called discretization error due to the piecewise approximation.

Using Taylor's backward series expansion,

$$u(x_i-\Delta x)|_{t_n} = u|_{x_i,t_n} - \Delta x \cdot \frac{\partial u}{\partial x}|_{x_i,t_n} + \frac{\Delta x^2}{2} \cdot \frac{\partial^2 u}{\partial x^2}|_{x_i,t_n} - \frac{\Delta x^3}{6} \cdot \frac{\partial^3 u}{\partial x^3}|_{x_i,t_n} + \frac{\Delta x^4}{24} \cdot \frac{\partial^4 u}{\partial x^4}|_{x_i\xi_1} \qquad 4.4$$

The error term is again attributed from a space point located between x_i and x_i - Δx . Adding Forward Difference to Backward Difference expansion, the following centered difference approximation is obtained:

$$\frac{\partial^2 u}{\partial x^2}|_{x_i,t_n} = \left[\frac{u(x_i+\Delta x) - 2u(x_i) + u(x_i-\Delta x)}{(\Delta x)^2}\right]_{t_n} + O[(\Delta x)^2] \qquad 4.5$$

where $O[(\Delta x)^2]$ is a shorthanded notation for the remainder term and global error, which approaches to zero as the space increment decreases . Equation above is commonly referred as a second-order accurate, centered-difference approximation to the second order spacial derivative of u. Let a subscript i represent the space position and a superscript n for the time observation point. Then, we obtain

$$\frac{\partial^2 u}{\partial x^2}\Big|_{x_i,t_n} = \left[\frac{u(x_i+\Delta x)^n - 2u(x_i)^n + u(x_i-\Delta x)^n}{(\Delta x)^2}\right]_{t_n} + O[(\Delta x)^2] \qquad 4.6$$

$$= \left[\frac{u_{i+1}^n - 2u_i^n + u_{i-1}^n}{(\Delta x)^2}\right]_{t_n} + O[(\Delta x)^2] \qquad 4.7$$

where

$u(x_i+\Delta x)^n = u_{i+1}^n$

$2u(x_i)^n = 2u_i^n$

$u(x_i-\Delta x)^n = u_{i-1}^n$

In Euation 4.7 and all subsequent finite-difference expressions, $u^n{}_i$ denotes a field quantity calculated at the space location $x_i = i\Delta x$ and the time point $t_n = n\Delta t$.

For the second partial time derivative, the space location, x_i is fixed and expand u in forward and backward Taylor's series in time. By analogy with the development of Equation 4.5 through 4.7 a second-order accurate centered-difference approximation to the second partial time derivative of u is obtained as follow:

$$\frac{\partial^2 u}{\partial x^2}\Big|_{x_i,t_n} = \left[\frac{u_i(t_n+\Delta t) - 2u_i(t_n)^n + u_i(t_n-\Delta t)}{(\Delta x)^2}\right]_{t_n} + O[(\Delta x)^2] \qquad 4.8$$

$$= \left[\frac{u_i^{n+1} - 2u_i^n + u_i^{n-1}}{(\Delta x)^2}\right]_{t_n} + O[(\Delta x)^2] \qquad 4.9$$

IV.2.3 Finite-Difference formulation of Maxwell's curl equation [15]

Basic ideas to obtain discrete approximations for the time-dependent Maxwell's electromagnetic curl equations for the lossless system, Yee's algorithm is introduced. The

Yee's algorithm is called "leapfrog" approach and uses the centered difference approximation for both electric and magnetic field solutions in time and space. This approach is robust because it uses Maxwell's dual curl equations to solve electric and magnetic field simultaneously rather than solving each field alone. As a result, that continuity of tangential magnetic field components, $\vec{H}_{tan}$ is automatically satisfied and the singularity of tangential magnetic field often occurring near edges and corner's of the conductor can be avoided and modeled efficiently. In addition, parameters for both of electric and magnetic materials can be implemented simultaneously.

Figure4.1 shows six electric and magnetic fields which form a unit cell. This unit cell is the basis of the FDTD numerical algorithm for the electric and magnetic field interactions in three dimensional system. The *x, y, z* dimensions of the unit cell are $i\Delta x$, $j\Delta y$, $k\Delta z$, respectively. Since centered difference is used, the notation, $(i\pm 1/2)$, $(j\pm 1/2)$ and $(k\pm 1/2)$ represent a half point of space step between i and $i\pm 1$, j and $j\pm 1$, and k and $k\pm 1$, respectively. This notation is directly implemented on the computer. The time steps are indicated with the subscript n. Similarly the half point of time step is denoted as $n\pm 1/2$.

Maxwell's curl equations, Equation 4.1 and 4.2 yields following six vector components to form the basis of the FDTD numerical algorithm for the time and spacial computational domain:

$$\frac{\partial H_x}{\partial t} = \frac{1}{\mu}\left(\frac{\partial E_y}{\partial z} - \frac{\partial E_z}{\partial y}\right) \qquad 4.10$$

$$\frac{\partial H_y}{\partial t} = \frac{1}{\mu}\left(\frac{\partial E_z}{\partial x} - \frac{\partial E_x}{\partial z}\right) \qquad 4.11$$

$$\frac{\partial H_z}{\partial t} = \frac{1}{\mu}\left(\frac{\partial E_x}{\partial y} - \frac{\partial E_y}{\partial x}\right) \qquad 4.12$$

$$\frac{\partial E_x}{\partial t} = \frac{1}{\varepsilon}\left(\frac{\partial H_z}{\partial y} - \frac{\partial H_y}{\partial z}\right) \tag{4.13}$$

$$\frac{\partial E_y}{\partial t} = \frac{1}{\varepsilon}\left(\frac{\partial H_x}{\partial z} - \frac{\partial H_z}{\partial x}\right) \tag{4.14}$$

$$\frac{\partial E_z}{\partial t} = \frac{1}{\varepsilon}\left(\frac{\partial H_y}{\partial x} - \frac{\partial H_x}{\partial y}\right) \tag{4.15}$$

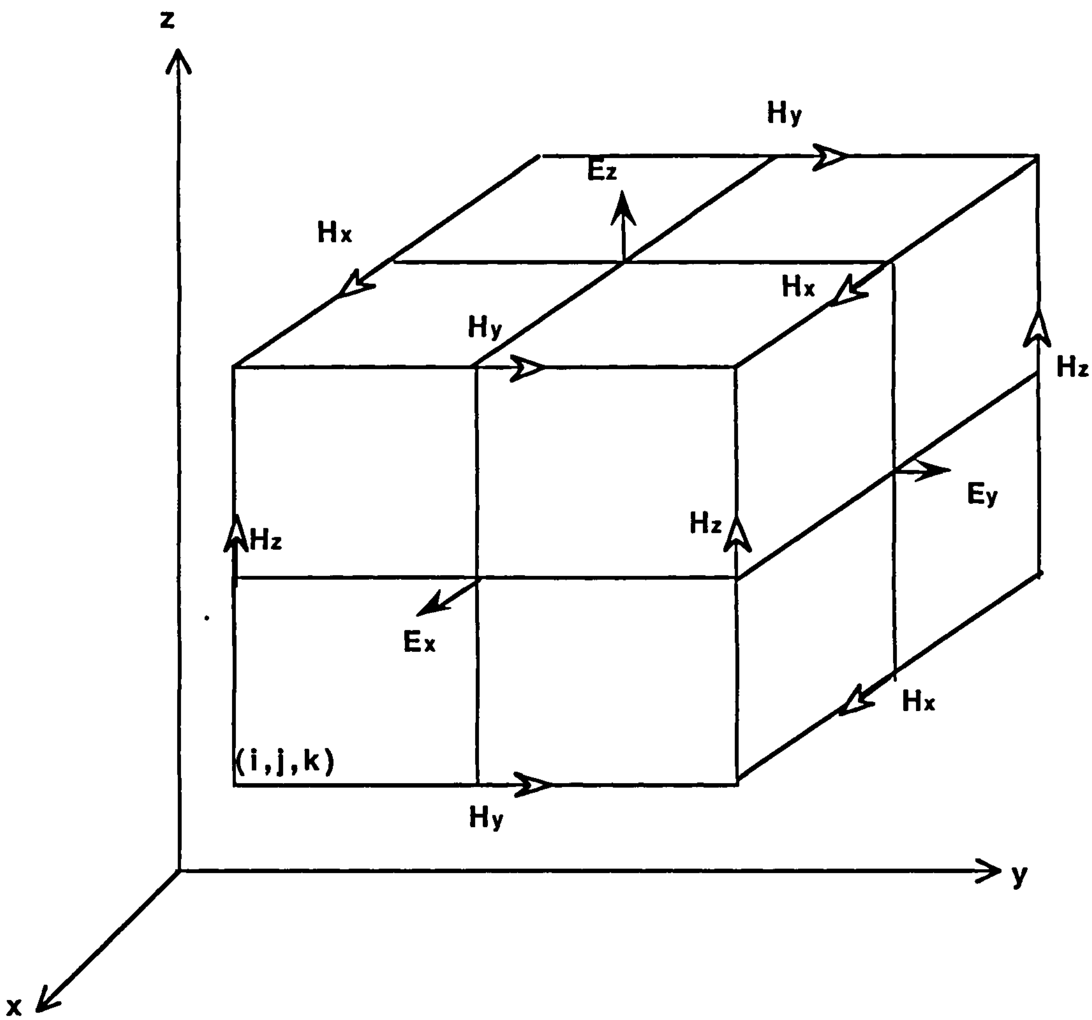

Figure 4.1 Position of the electric and magnetic field vector components about a cubic unit cell of the Yee space lattice [15,18]

Using Yee's algorithm for the centered difference approximation on both the time and space first-order differential equations and substituting n for the time steps and (i, j, k) for the spacial lattice point, Equation 4.10 is represented as follow:

$$\frac{\partial H_x}{\partial t} = \frac{H_x\Big|_{i,j+1/2,k+1/2}^{n+1/2} - H_x\Big|_{i,j+1.2,k+1/2}^{n-1/2}}{\Delta t}$$

$$-\frac{1}{\mu}\left(\frac{\partial E_y}{\partial z} - \frac{\partial E_z}{\partial y}\right) = -\frac{1}{\mu}\left[\left(\frac{E_y\Big|_{i,j+1.2,k+1}^{n+1/2} - E_y\Big|_{i,j+1.2,k}^{n+1/2}}{\Delta z}\right) - \left(\frac{E_z\Big|_{i,j+1,k+1/2}^{n+1/2} - E_z\Big|_{i,j,k+1/2}^{n+1/2}}{\Delta y}\right)\right] \quad 4.16$$

therefore,

$$\frac{H_x\Big|_{i,j+1/2,k+1/2}^{n+1/2} - H_x\Big|_{i,j+1.2,k+1/2}^{n-1/2}}{\Delta t}$$

$$= -\frac{1}{\mu}\left[\left(\frac{E_y\Big|_{i,j+1/2,k+1}^{n} - E_y\Big|_{i,j+1.2,k}^{n}}{\Delta z}\right) - \left(\frac{E_z\Big|_{i,j+1,k+1/2}^{n} - E_z\Big|_{i,j,k+1/2}^{n}}{\Delta y}\right)\right]$$

4.17

$$H_x\Big|_{i,j+1/2,k+1/2}^{n+1/2}$$

$$= H_x\Big|_{i,j+1/2,k+1/2}^{n-1/2} - \frac{\Delta t}{\mu}\left[\left(\frac{E_y\Big|_{i,j+1/2,k+1}^{n} - E_y\Big|_{i,j+1.2,k}^{n}}{\Delta z}\right) - \left(\frac{E_z\Big|_{i,j+1,k+1/2}^{n} - E_z\Big|_{i,j,k+1/2}^{n}}{\Delta y}\right)\right] \quad 4.18$$

similarly,

$$H_y\Big|_{i+1/2,j,k+1/2}^{n+1/2}$$

$$= H_y\Big|^{n-1/2}_{i+1/2,j,k+1/2} - \frac{\Delta t}{\mu}\left[\left(\frac{E_x\Big|^{n}_{i+1/2,j,k+1} - E_x\Big|^{n}_{i+1/2,j,k}}{\Delta z}\right) - \left(\frac{E_z\Big|^{n}_{i+1,j,k+1/2} - E_z\Big|^{n}_{i,j,k+1/2}}{\Delta x}\right)\right] \qquad 4.19$$

$$H_z\Big|^{n+1/2}_{i+1/2,j+1/2,k}$$

$$= H_y\Big|^{n-1/2}_{i+1/2,j+1/2,k} - \frac{\Delta t}{\mu}\left[\left(\frac{E_y\Big|^{n}_{i+1,j+1/2,k} - E_y\Big|^{n}_{i,j+1/2,k}}{\Delta x}\right) - \left(\frac{E_x\Big|^{n}_{i+1/2,j+1,k+1/2} - E_x\Big|^{n}_{i/2,j,k+1/2}}{\Delta y}\right)\right] \qquad 4.20$$

$$E_x\Big|^{n+1}_{i+1/2,j,k}$$

$$= E_x\Big|^{n}_{i+1/2,j,k} + \frac{\Delta t}{\varepsilon}\left[\left(\frac{H_z\Big|^{n+1/2}_{i+1/2,j+1/2,k} - H_z\Big|^{n+1/2}_{i,j-1/2,k}}{\Delta y}\right) - \left(\frac{H_y\Big|^{n+1/2}_{i+1/2,j,k+1/2} - H_y\Big|^{n+1/2}_{i+1/2,j,k-1/2}}{\Delta z}\right)\right] \qquad 4.21$$

$$E_y\Big|^{n+1}_{i,j+1/2,k}$$

$$= E_y\Big|^{n}_{i,j+1/2,k} + \frac{\Delta t}{\varepsilon}\left[\left(\frac{H_x\Big|^{n+1/2}_{i,j+1/2,k+1/2} - H_x\Big|^{n+1/2}_{i,j+1/2,k-1/2}}{\Delta z}\right) - \left(\frac{H_z\Big|^{n+1/2}_{i+1/2,j+1/2,k} - H_z\Big|^{n+1/2}_{i-1/2,j+1/2,k}}{\Delta x}\right)\right]$$

4.22

$$E_z\Big|^{n+1}_{i,j,k+1/2}$$

$$= E_z\Big|^{n}_{i,j,k+1/2} + \frac{\Delta t}{\varepsilon}\left[\left(\frac{H_y\Big|^{n+1/2}_{i+1/2,j,k+1/2} - H_y\Big|^{n+1/2}_{i-1/2,j,k+1/2}}{\Delta x}\right) - \left(\frac{H_x\Big|^{n+1/2}_{i,j+1/2,k+1/2} - H_x\Big|^{n+1/2}_{i,j-1/2,k+1/2}}{\Delta y}\right)\right] \qquad 4.23$$

As shown in Equation 4.18 through Equation 4.23 the new value of the field vector is obtained from the adjacent space and previous time steps. Therefore, at any given space and time step only one point at a time is computed.

IV.2.4 Stability Consideration [15]

To reduce the spurious numerical results and to minimize numerical errors, the space increments Δx, Δy and Δz, and the time increment Δt have to be chosen such that the numerical unstability should be avoided and the numerical dispersion has to be reduced. In other words, Δt must be bounded to Δx, Δy and Δz to maintain the stability of numerical solutions. The following section describes how stability algorithm is developed from the Maxwell's curl equations in three dimensional space and shows how the time increment Δt is bound to the space increments Δx, Δy and Δz.

To derive the stability factor, all six vector components Hx, Hy, Hz, Ex, Ey and Ez represented by Equation 4.10 through 4.15 are isolated for time and space to set as an eigenvalue problems. First, the time eigenvalue problem is considered. Assuming all the electricfield Ex, Ey and Ez, and magnetic field Hx, Hy and Hz belong to a generic field vector component Ψ. Then discretized Ψ in the time and three dimensional space.

$$\frac{\Psi|_{i,j,k}^{n+1/2} - \Psi|_{i,j,k}^{n-1/2}}{\Delta t} = \Lambda \Psi|_{i,j,k}^{n} \quad \text{and let } \alpha|_{i,j,k} = \frac{\Psi|_{i,j,k}^{n+1/2}}{\Psi|_{i,j,k}^{n}} = \frac{\Psi|_{i,j,k}^{n}}{\Psi|_{i,j,k}^{n-1/2}} \qquad 4.24$$

Stability algorithm requires $\left|\alpha|_{i,j,k}\right| \leq 1$ for all possible spatial modes in the mesh and for all points i, j and k. Substituting $\alpha|_{i,j,k}$ into Equation 4.24

$$\frac{\left(\alpha|_{i,j,k}\Psi|_{i,j,k}^{n}\right) - \left(\Psi|_{i,j,k}^{n} / \alpha|_{i,j,k}\right)}{\Delta t} = \Lambda \Psi|_{i,j,k}^{n} \qquad 4.25$$

After factoring out $\Psi|_{i,j,k}^{n}$ the following quadradic equation is obtained:

$$\frac{\left(\alpha|_{i,j,k}\right)^2-1}{\alpha|_{i,j,k}\Delta t}=\Lambda \text{ Rearranging it } \left(\alpha|_{i,j,k}\right)^2-\Delta t\Lambda\alpha|_{i,j,k}-1=0 \qquad 4.26$$

To solve $\alpha|_{i,j,k}$ the quadradic formula is used:

$$\alpha|_{i,j,k}=\frac{\Lambda\Delta t\pm\sqrt{(\Lambda\Delta t)^2+4}}{2}$$

$$=\frac{\Lambda\Delta t}{2}+\sqrt{\left(\frac{\Lambda\Delta t}{2}\right)^2+1} \qquad 4.27$$

Let $b=\dfrac{\Lambda\Delta t}{2}$

then $\sqrt{\left(\dfrac{\Lambda\Delta t}{2}\right)^2+1}=\sqrt{b^2+1}$ 4.28

If b is pure imaginary and bound between -j1 and j1, $-j1\le b\le j1$ the above quadratic solution for $\alpha|_{i,j,k}$ always satisfies $\left|\alpha|_{i,j,k}\right|\le 1$. Then $\left|\alpha|_{i,j,k}\right|=\sqrt{\left(b^2+\sqrt{b^2+1}^2\right)}\le 1$. Since

$-1\le \mathrm{Im}(b)=\mathrm{Im}(\dfrac{\Lambda\Delta t}{2})\le 1$ and $-1\le \mathrm{Im}(\dfrac{\Lambda\Delta t}{2})\le 1$, therefore, $-\dfrac{2}{\Delta t}\le \mathrm{Im}(\Lambda)\le\dfrac{2}{\Delta t}$. 4.29

Next the algorithm stability requirement for the space discritization is considered. Rewriting Maxwell's curl equation for the lossless system and for the simplicity, letting *u=1* and ε=1 yield following equations:

$$\nabla\times\mathrm{E}=-\frac{\partial\mathrm{H}}{\partial t}=(j)^2\frac{\partial\mathrm{H}}{\partial t} \text{ and } j\nabla\times\mathrm{H}=j\frac{\partial\mathrm{E}}{\partial t} \qquad 4.30$$

$$j\nabla\times(\mathrm{H}+j\mathrm{E})=j\frac{\partial\mathrm{E}}{\partial t}+\frac{\partial\mathrm{H}}{\partial t}=\frac{\partial}{\partial t}(\mathrm{H}+j\mathrm{E}) \qquad 4.31$$

Substituting $\mathrm{H}+j\mathrm{E}=\Psi$ into Equation 4.27 gives $j\nabla\times\Psi=\dfrac{\partial\Psi}{\partial t}$. This can be set as an eigenvalue problem: $j\nabla\times\Psi=\dfrac{\partial\Psi}{\partial t}=\Lambda\Psi$ 4.32

Say $\Psi = \Psi_0 e^{j(\tilde{k}_x I\Delta x + \tilde{k}_y J\Delta y + \tilde{k}_z K\Delta z)}$ where I, J and K are corresponding to the coordinate node numbers in the x, y and z direction s in the spacial frequency domain. $\tilde{k}_x$, $\tilde{k}_y$ and $\tilde{k}_z$ are wave numbers in the same domain. $j\nabla \times \Psi = j\left(\hat{x}\frac{\partial}{\partial x} + \hat{y}\frac{\partial}{\partial y} + \hat{z}\frac{\partial}{\partial z}\right) \times \Psi$. The curl operator can be expressed with the centered difference discretization:

$$j\left(\hat{x}\frac{\partial}{\partial x} + \hat{y}\frac{\partial}{\partial y} + \hat{z}\frac{\partial}{\partial z}\right)\Psi = j\left(\hat{x}\frac{\partial \Psi}{\partial x} + \hat{y}\frac{\partial \Psi}{\partial y} + \hat{z}\frac{\partial \Psi}{\partial z}\right) \qquad 4.33$$

$$\hat{x}\frac{\partial \Psi}{\partial x} = \hat{x}\frac{\Psi_0}{\Delta x}\left(e^{j(\tilde{k}_x(I+1/2)\Delta x + \tilde{k}_y J\Delta y + \tilde{k}_z K\Delta z)} - e^{j(\tilde{k}_x(I-1/2)\Delta x + \tilde{k}_y J\Delta y + \tilde{k}_z K\Delta z)}\right)$$

$$= \hat{x}\frac{\Psi_0}{\Delta x}\left(e^{j\frac{\tilde{k}_x \Delta x}{2}} - e^{j\frac{\tilde{k}_x \Delta x}{2}}\right)e^{j(\tilde{k}_x \Delta x + \tilde{k}_y J\Delta y + \tilde{k}_z K\Delta z)} \qquad 4.34$$

Factoring out $e^{j(\tilde{k}_x I\Delta x + \tilde{k}_y J\Delta y + \tilde{k}_z K\Delta z)}$ and using Euler's Identity we obtain

$\hat{x}\frac{\partial \Psi}{\partial x} = \hat{x}\frac{\Psi_0}{\Delta x}2j\sin\left(\frac{\tilde{k}_x \Delta x}{2}\right)$ similarly solving for $\hat{y}$ and $\hat{z}$ then

$$j\nabla \times \Psi = -2\left[\hat{x}\frac{\Psi_0}{\Delta x}j\sin\left(\frac{\tilde{k}_x \Delta x}{2}\right) + \hat{y}\frac{\Psi_0}{\Delta y}j\sin\left(\frac{\tilde{k}_x \Delta y}{2}\right) + \hat{z}\frac{\Psi_0}{\Delta z}j\sin\left(\frac{\tilde{k}_x \Delta z}{2}\right)\right] = \Lambda\Psi \qquad 4.35$$

This result is from the discretization of Ψ

$$\text{Let } \vec{A} = -2\left[\hat{x}\frac{\Psi_0}{\Delta x}j\sin\left(\frac{\tilde{k}_x \Delta x}{2}\right) + \hat{y}\frac{\Psi_0}{\Delta y}j\sin\left(\frac{\tilde{k}_x \Delta y}{2}\right) + \hat{z}\frac{\Psi_0}{\Delta z}j\sin\left(\frac{\tilde{k}_x \Delta z}{2}\right)\right] \qquad 4.36$$

Then, $j\nabla \times \Psi = j\vec{A} \times \Psi = \Lambda\Psi$. This holds true because Ψ is a complex function.

and squaring both sides

$$\left(j\vec{A} \times \Psi\right)^2 = -\left|\vec{A}\right|^2 |\Psi|^2 \qquad 4.37$$

Using vector identity gives $\left(\vec{A} \times \Psi\right)^2 = \left|\vec{A}\right|^2 |\Psi|^2$. 4.38

from the right hand side, $(\Lambda\Psi)^2 = \Lambda^2 |\Psi|^2$. $-\left|\vec{A}\right|^2 = \Lambda^2$ 4.39

Therefore,

$$\Lambda^2 = -4\left[\frac{1}{(\Delta x)^2}(\sin)^2\left(\frac{\tilde{k}_x \Delta x}{2}\right) + \frac{1}{(\Delta y)^2}(\sin)^2\left(\frac{\tilde{k}_y \Delta y}{2}\right) + \frac{1}{(\Delta z)^2}(\sin)^2\left(\frac{\tilde{k}_z \Delta z}{2}\right)\right] \qquad 4.40$$

Since Λ is imaginary and for all possible $\tilde{k}_x$, $\tilde{k}_y$ and $\tilde{k}_z$, sin(max)=1,

$$-2\sqrt{\frac{1}{(\Delta x)^2}+\frac{1}{(\Delta y)^2}+\frac{1}{(\Delta z)^2}} \le \mathrm{Im}(\Lambda) \le 2\sqrt{\frac{1}{(\Delta x)^2}+\frac{1}{(\Delta y)^2}+\frac{1}{(\Delta z)^2}} \qquad 4.41$$

The range of eigenvalues set by eq(41) guarantees the numerical stability for the spacial modes. To guarantee the numerical stability for the time stepping, the range of eigenvalues obtained in Equation 4.29 has to be satisfied.

Combining Equation 4.29, $-\frac{2}{\Delta t} \le \mathrm{Im}(\Lambda) \le \frac{2}{\Delta t}$ and 5.41 yields

$$\Delta t \le \sqrt{\frac{1}{(\Delta x)^2}+\frac{1}{(\Delta y)^2}+\frac{1}{(\Delta z)^2}} \qquad 4.42$$

Since the imaginary eigenvalue is symmetrical about the zero the upper bound is only considered in Equation 4.42. This relationship guarantees the numerical stability and avoids spurious result without limit as time marches. In this numerical analysis the cubic lattice *Δx=Δy=Δz=Δ* is used, denormzlizing to a nonunity value of c (speed of light), therefore Equation 4.42 is further simplified:

$$\Delta t \le \frac{1}{c\sqrt{\frac{3}{\Delta^2}}} = \frac{\Delta}{c\sqrt{3}} \qquad 4.43$$

IV.2.5 Source Excitation [20]

A Gaussian electric field pulse is used to simplify the excitation by setting the fields to zero at *t=0* in the computational domain. By setting *Ey=Ez=0* only Ex component (perpendicular to the surface of microstrip) is excited near the input port to minimize the reflection resulted from the imperfect absorbing boundary condition. The Gaussian pulse is generally used to provide the frequency spectrum from dc to the frequency of interest by adjusting pulse width. The Gaussian pulse is represented as follow:

$$E_x(t) = e^{-\frac{(t-t_0)^2}{T^2}} \qquad 4.44$$

Time discretization is performed with the following time steps and sequence:

where $t = n \cdot \Delta t \qquad n = 1 \sim 2000$

$t_0 = 250 \cdot \Delta t \qquad \Delta t = 9.63 \times 10^{-14}$

$\frac{t_0}{T} = 2.5$

The time step is chosen based on the stability criterion to insure the stability of numerical analysis. Particularly to avoid numerical dispersions, the time and space steps have to be carefully chosen. Otherwise the velocity of propagation can be varied as a function of frequency even for the TEM modes. This deviates from the accurate analysis. It has been reported [17]that this numerical dispersion and truncation error can be minimized if a maximum step size is chosen to be less than 1/20th of the wave length of the highest cutoff frequency of interest.

IV.2.6 Conductor Treatment

In this simulation, all transmission lines are treated as Perfect Electric Conductors(PEC) with zero thickness. In this case, total tangential electric field on the surface of the PEC is assumed to be zero. Therefore, $E_{\tan}|_{tot} = 0$ and $E_{\tan}|_{ref} = -E_{\tan}|_{inc}$. Since this approximation is an analytical expression it does not force to generate the numerical errors. The magnetic field on the surface is also assumed to be zero but infinitely large current density is required to satisfy the boundary condition. Therefore the current per unit width along the surface of the PEC is equal to the magnetic strength just out side the surface of the PEC. This is: $-J_s = H_{\tan}|_{outside}$ The magnetic field and surface current will be parallel to the surface, but perpendicular to each other. The current is the cross product of a unit vector along the outward normal to the surface and the magnetic field just outside of the PEC: $J_s = \hat{n} \times \mathrm{H}$.

IV.2.7 Boundary Condition [15,16]

For the boundary condition, Mur's second order absorbing boundary condition is used. Applying an appropriate boundary condition is the key for obtaining desired analysis in the FDTD analysis. Particularly, for all time steps, the reflected wave from the boundary condition should be negligibly small to be allowed in the vicinity of the structure of interest. Since the computational domain is limited in the FDTD analysis, the size and boundary condition of computation domain have to be chosen such that the results should be sufficiently accurate enough to analyze the structure of interest.

The tangential electric field component is continuous; however, at the boundary where the computational domain ends the tangential electric field should be either radiated to the open boundary or absorbed by the absorbing boundary so that it does not reflect back to the structure of interest. In this work, only absorbing boundary condition is considered. Outside the computational domain the field can not be evaluated. Therefore, it requires some special scheme at the boundary to minimize the reflection. For the special scheme the second order absorbing boundary condition introduced by Mur (ref)is shown as follow:

$$x=0 \quad \frac{\partial^2 U}{\partial x \partial t} - \frac{1}{c}\frac{\partial^2 U}{\partial t^2} + \frac{c}{2}\frac{\partial^2 U}{\partial y^2} + \frac{c}{2}\frac{\partial^2 U}{\partial z^2} = 0 \qquad 4.45$$

$$x=h \quad \frac{\partial^2 U}{\partial x \partial t} + \frac{1}{c}\frac{\partial^2 U}{\partial t^2} - \frac{c}{2}\frac{\partial^2 U}{\partial y^2} - \frac{c}{2}\frac{\partial^2 U}{\partial z^2} = 0 \qquad 4.46$$

$$y=0 \quad \frac{\partial^2 U}{\partial y \partial t} - \frac{1}{c}\frac{\partial^2 U}{\partial t^2} + \frac{c}{2}\frac{\partial^2 U}{\partial x^2} + \frac{c}{2}\frac{\partial^2 U}{\partial z^2} = 0 \qquad 4.47$$

$$y=h \quad \frac{\partial^2 U}{\partial y \partial t} + \frac{1}{c}\frac{\partial^2 U}{\partial t^2} - \frac{c}{2}\frac{\partial^2 U}{\partial x^2} - \frac{c}{2}\frac{\partial^2 U}{\partial z^2} = 0 \qquad 4.48$$

$$z=0 \quad \frac{\partial^2 U}{\partial z \partial t} - \frac{1}{c}\frac{\partial^2 U}{\partial t^2} + \frac{c}{2}\frac{\partial^2 U}{\partial x^2} + \frac{c}{2}\frac{\partial^2 U}{\partial y^2} = 0 \qquad 4.49$$

$$z=h \quad \frac{\partial^2 U}{\partial z \partial t} + \frac{1}{c}\frac{\partial^2 U}{\partial t^2} - \frac{c}{2}\frac{\partial^2 U}{\partial x^2} - \frac{c}{2}\frac{\partial^2 U}{\partial y^2} = 0 \qquad 4.50$$

where $x=0$, $x=h$, $y=0$, $y=h$ and $z=0$, $z=h$ are the boundaries of the computational domain. Then using the centered finite difference and let $U\big|_{i,j,0}^{n}$ represent a tangential electric field at the boundary $z=0$. From equation Equation 4.49 the field at $1/2$ space steps of z coordinate can be evaluated with the mixed x and t derivatives:

$$\begin{aligned}\left.\frac{\partial^2 U}{\partial z \partial t}\right|_{i,j,1/2}^{n} &= \frac{1}{2\Delta t}\left(\left.\frac{\partial U}{\partial z}\right|_{i,j,1/2}^{n+1} - \left.\frac{\partial U}{\partial z}\right|_{i,j,1/2}^{n-1}\right) \\ &= \frac{1}{2\Delta t}\left[\left(\frac{U\big|_{i,j,1}^{n+1} - U\big|_{i,j,0}^{n+1}}{\Delta z}\right) - \left(\frac{U\big|_{i,j,1}^{n-1} - U\big|_{i,j,0}^{n-1}}{\Delta z}\right)\right] \qquad 4.51\end{aligned}$$

The second order partial derivatives with respect time is expressed as the average point of $(i, j, 0)$ and $(i, j, 1)$:

$$\begin{aligned}\left.\frac{\partial^2 U}{\partial t^2}\right|_{i,j,1/2}^{n} &= \frac{1}{2}\left(\left.\frac{\partial^2 U}{\partial t^2}\right|_{i,j,0}^{n} + \left.\frac{\partial^2 U}{\partial t^2}\right|_{i,j,1}^{n}\right) \\ &= \frac{1}{2}\left[\left(\frac{U\big|_{i,j,0}^{n+1} - 2U\big|_{i,j,0}^{n} + U\big|_{i,j,0}^{n-1}}{(\Delta t)^2}\right) + \left(\frac{U\big|_{i,j,1}^{n+1} - 2U\big|_{i,j,1}^{n} + U\big|_{i,j,1}^{n-1}}{(\Delta t)^2}\right)\right] \qquad 4.52\end{aligned}$$

Similarly, the second order partial derivative with respect to x is obtained from the average point of adjacent points of x and z coordinates:

$$\left.\frac{\partial^2 U}{\partial x^2}\right|_{i,j,1/2}^{n} = \frac{1}{2}\left(\left.\frac{\partial^2 U}{\partial x^2}\right|_{i,j,0}^{n} + \left.\frac{\partial^2 U}{\partial x^2}\right|_{i,j,1}^{n}\right)$$

$$= \frac{1}{2}\left[\left(\frac{U|_{i+1,j,0}^{n} - 2U|_{i,j,0}^{n} + U|_{i-1,j,0}^{n}}{(\Delta x)^2}\right) + \left(\frac{U|_{i+1,j,1}^{n} - 2U|_{i,j,1}^{n} + U|_{i-1,j,1}^{n}}{(\Delta x)^2}\right)\right] \quad 4.53$$

Similarly, for the second y derivative is expressed:

$$\left.\frac{\partial^2 U}{\partial y^2}\right|_{i,j,1/2}^{n} = \frac{1}{2}\left(\left.\frac{\partial^2 U}{\partial y^2}\right|_{i,j,0}^{n} + \left.\frac{\partial^2 U}{\partial y^2}\right|_{i,j,1}^{n}\right)$$

$$= \frac{1}{2}\left[\left(\frac{U|_{i,j+1,0}^{n} - 2U|_{i,j,0}^{n} + U|_{i,j-1,0}^{n}}{(\Delta y)^2}\right) + \left(\frac{U|_{i,j+1,1}^{n} - 2U|_{i,j,1}^{n} + U|_{i,j-1,1}^{n}}{(\Delta y)^2}\right)\right] \quad 4.54$$

Solving for the $U|_{i,j,0}^{n+1}$ by substituting the centered expressions into Equation 4.49 yields the following expression for the consecutive time steps:

Let the spacial increment(Δ) is uniform in the x, y and z directions,

$$U|_{i,j,0}^{n+1} = -U|_{i,j,0}^{n-1} + \frac{c\Delta t - \Delta}{c\Delta t + \Delta}\left(U|_{i,j,1}^{n+1} + U|_{i,j,0}^{n-1}\right)$$

$$+ \frac{2\Delta}{c\Delta t + \Delta}\left(U|_{i,j,1}^{n} + U|_{i,j,0}^{n}\right)$$

$$+ \frac{(c\Delta t)^2}{2\Delta(c\Delta t + \Delta)}\begin{pmatrix} U|_{i,j+1,0}^{n} - 2U|_{i,j,0}^{n} + U|_{i,j-1,0}^{n} \\ +U|_{i,j+1,1}^{n} - 2U|_{i,j,1}^{n} + U|_{i,j-1,1}^{n} \end{pmatrix}$$

$$+ \frac{(c\Delta t)^2}{2\Delta(c\Delta t + \Delta)}\begin{pmatrix} U|_{i+1,j,0}^{n} - 2U|_{i,j,0}^{n} + U|_{i-1,j,0}^{n} \\ +U|_{i+1,j,1}^{n} - 2U|_{i,j,1}^{n} + U|_{i-1,j,1}^{n} \end{pmatrix}$$

$$+ \frac{(c\Delta t)^2}{2\Delta(c\Delta t + \Delta)}\begin{pmatrix} U|_{i+1,j,0}^{n} - 2U|_{i,j,0}^{n} + U|_{i-1,j,0}^{n} \\ +U|_{i+1,j,1}^{n} - 2U|_{i,j,1}^{n} + U|_{i-1,j,1}^{n} \end{pmatrix} \quad 4.55$$

At $z=h$ the following centered finite difference expression is obtained:

$$
\begin{aligned}
U\big|_{i,j,k}^{n+1} = & -U\big|_{i,j,k}^{n-1} + \frac{c\Delta t - \Delta}{c\Delta t + \Delta}\left(U\big|_{i,j,k}^{n+1} + U\big|_{i,j,k-1}^{n-1}\right) \\
& + \frac{2\Delta}{c\Delta t + \Delta}\left(U\big|_{i,j,k}^{n} + U\big|_{i,j,k-1}^{n}\right) \\
& + \frac{(c\Delta t)^2}{2\Delta(c\Delta t + \Delta)}\begin{pmatrix} U\big|_{i,j+1,k}^{n} - 2U\big|_{i,j,k}^{n} + U\big|_{i,j-1,k}^{n} \\ +U\big|_{i,j+1,k-1}^{n} - 2U\big|_{i,j,k-1}^{n} + U\big|_{i,j-1,k-1}^{n} \end{pmatrix} \\
& + \frac{(c\Delta t)^2}{2\Delta(c\Delta t + \Delta)}\begin{pmatrix} U\big|_{i+1,j,k}^{n} - 2U\big|_{i,j,k}^{n} + U\big|_{i-1,j,k}^{n} \\ +U\big|_{i+1,j,k-1}^{n} - 2U\big|_{i,j,k-1}^{n} + U\big|_{i-1,j,k-1}^{n} \end{pmatrix}
\end{aligned}
\qquad 4.56
$$

Above Mur ABCs scheme permits the average of 1%~ 5% spurious reflection in the numerical analysis.

CHAPTER V. APPLICATION OF FDTD TO COUPLED MICROTRIP LINES

In order to verify the general applicability of FDTD method to determine various parameters [21,22,23] associated with microwave circuit elements, a coupled microstrip line is chosen. This choice is based on the premise that all parameters of coupled microstrip lines have been determined by various calculational methods and have also been experimentally tested. Using these results, microwave circuits such as various filters have been thoroughly designed and experimentally verified.

In this work,:

- scattering parameters,
- odd(Z_{0o})-even(Z_{0e}) impedances
- coupling coefficient and
- lumped equivalent circuit model

are calculated from the FDTD simulations of coupled microstrip lines. These parameters are then compared to existing solutions on microstrip lines and in certain cases experimentally tested. Especially,using a full vector electric and magnetic field FDTD analysis, an unique approach to develop an equivalent circuit of the coupled line is discussed.

V.1 MICROWAVE PARAMETERS

Figure 5.1 shows the schematic representation of coupled microstrip lines. Here the lines widths are w, the separation between the strips is s, the height of the substrate is h. Dimensions used for the simulations will be given in the latter sections. Calculation of the various parameters are described in the next subsections.

V.1.1 Characteristic Impedance and Scattering Parameters

FDTD analysis provides full-vector electric and magnetic field distributions in time and space. Therefore, all microwave circuit parameters in the frequency domain can be obtained from the simple Fourier transform of the transient wave.

Since quasi-TEM mode is assumed in this study, the static field solution is obtained as a solution to the Laplace's equation:

$$\nabla^2 \cdot V = 0 \qquad 5.1$$

Therefore the voltage can be simply obtained by integrating vertical electric field from the ground plane to the surface of the conductor by the line integral

$$V(z,t) = \int_{c_v} \vec{E}(x_i, y_i, z, t) \cdot d\vec{l}_i . \qquad 5.2$$

Here, C_v indicates a path extending from the ground to the circuit location z. Similarly the current is calculated by integrating the transverse magnetic field around the conductor surface. The expression for the current is :

$$I(z,t) = \oint_{c_i} \vec{H}(x_i, y_i, z, t) \cdot d\vec{l}_i \qquad 5.3$$

The characteristic impedance, Z_0 is calculated from the ratio between the voltage and current:

$$Z_0(\omega, z) = \frac{F\{V(z,t)\}}{F\{I(z,t)\}} \qquad 5.4$$

where $\omega=2\pi f$, the angular frequency.

This derivation of impedance is based on the ratio between the voltage and current calculated from the corresponding electric and magnetic fields in time and space. However, Yee's leapfrog grid offsets the electric and magnetic fields by $\Delta/2$ in time and space. To compensate for this deviation, the voltage has to be spatially interpolated as [21]:

$$V|_{i,j,k} = \sqrt{V|_{i+1/2,j,k} V|_{i-1/2,j,k}} \qquad 5.5$$

The half time step can be compensated by introducing a multiplying a factor of $e^{-j\omega\Delta t/2}$ to the Fourier transformed current. Therefore Eq(6.4) becomes:

$$Z_0(\omega,z) = \frac{F\{\sqrt{V(z_{+1/2},t)V(z_{-1/2},t)}\}}{F\{I(z,t)\} \cdot e^{-j\omega\Delta t/2}} \qquad 5.7$$

However, if the fundamental mode is no longer valid in the system, the values for the voltage and current based on quasi-TEM mode is no longer accurate.

The frequency-dependent scattering parameters, $S_{i,k}$ are obtained typically from thevoltage ratio of reflected(where $i=k$), or transmitted to incident waves (where $i \neq k$).

$$S_{ii}(\omega) = \frac{F\{V_{ri}(t)\}}{F\{V_i(t)\}} \;;\; S_{ik}(\omega) = \frac{F\{V_{tk}(t)\}}{F\{V_i(t)\}} \text{ for } i \neq k \qquad 5.8$$

where $V_i(t)$, and $V_{ri}(t)$ are the incident and reflected at port i, respectively and $V_{ti}(t)$ is the transmitted wave at port k.

V.1.2 Even and Odd Mode Impedances [24]

The coupled lines of Figure 5.1 are assumed to be identical and are located at the same height with reference to the ground plane and the surrounding environment. Since three conductors(two signal lines and one ground plane) are involved in the system, the general field distribution of propagation mode can be represented as a superposition of two fundamental modes. The simplest choice of these two modes are even and odd modes.

The electric field of even mode is symmetrical to the center line (symmetry plane), and electric field component in the horizontal dirction vanishes at the symmetry plane. For the odd mode, the electric field distribution has an antisymmetry plane at the center line, and the antisymmetry plane has the same potential as the same potential as the ground plane. With these features, the FDTD was implemented to calculate the the characteristic impedance for the even and odd modes.

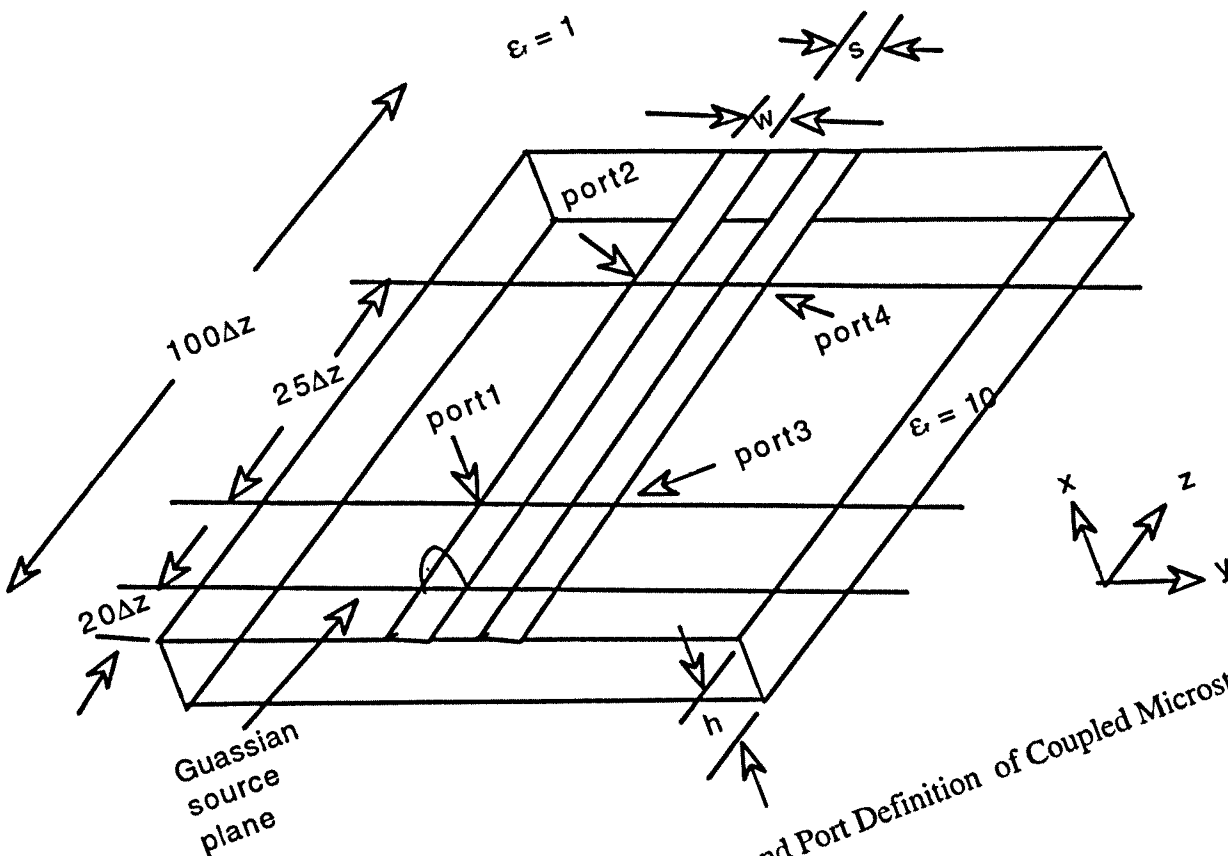

Figure 5.1 Source Excitation Point and Port Definition of Coupled Microstrip Line

V.1.3 Coupling Coefficient [8,24]

The coupling coefficient is a ratio of the difference to the sum of the even and odd characteristic impedances:

$$C = \frac{Z_c^e - Z_c^o}{Z_c^e + Z_c^o} \qquad 5.9$$

V.2. SIMULATION RESULTS

The two conductors of the coupled microsrip lines shown in Figure 5.1 are treated as perfect electric conductors (PEC) with zero thickness. The conductor lines, the substrate and the space above the lines (air) are enclosed in a box with six surrounding walls. The five walls except the bottom wall are treated with Mur's second order absorbing boundary condition to minimize the reflection from the walls. The bottom wall is treated as a perfect electric conductor to serve as the ground plane.

Simulation of these coupled microstrip lines involves the previously described application of the centered finite-difference equations of Maxwell's curl equations, source and boundary conditions. The space increment, $\Delta x=\Delta y=\Delta z=\Delta$ is chosen less than 1/20th of the wavelength of the highest frequency of interest. In order to simulate correctly, Δ is selected so that an integral number of nodes exactly fits the dimensions of the structures. Therefore, the width and spacing of the conductor, and the thickness of the substrate are chosen to compensate these requirements.

The space increment, $\Delta=50um$ is used in these simulations. The width and spacing of the conductor lines are 500*um* and 500*um*, respectively. The thickness of the substrate is 500*um* and the air thickness is 3000*um*. The total number of mesh points is 70x150x100. The source is exited just under the conductor at $20\Delta z$ on the *xy* plane. The observation points of $E_x(x,y,z,t)$ are selected at $z=70\Delta z$, $75\Delta z$, $80\Delta z$, $85\Delta z$ and $95\Delta z$, The time step Δt=.0963 *ps* is used. The Guassian half-width is T=100Δt and the time delay t_0 is set to be 250 Δt. This allows to start the Gaussian pulse with negligible electric field at t=0. The E_x electric fields are simulated for 2000 time steps. It took about 2-3 minutes for the computation of this simulation on Cray C90 super computer.

V.2.1 Fields of coupled lines

Figure 5.2 through 5.6 show the spatial distribution of $E_x(y,z,t)$ at x position just underneath the coupled microstrip lines at 200, 400, 600, 800 and 1000 time steps. These time marching electric fields show how the Guassian pulse propagates as time increases. As shown in Figure 5.2 the Gaussian pulse at 20Δz, the source plance of one conductor starts rising to propagate to both forward and backward z directions. Figure 5.3 shows both directions of propagation at 400 time steps. The field which is marching backward to the computation domain boundary is assumed to be absorbed with minimal reflection. At 600 time steps, Figure 5.4 shows the forward field marches without any interference from any reflection from the computation domain boundary. Figure 5.5 shows clearly the field has coupled to the other conductor line. Finally, at 1000 time steps the field is coupled to the other conductor line significantly, as shown in Figure 5.6. However, it would alos be interesting to find out if the length of the conductor lines are long enough eventually all fields may be coupled to the other line and consequently the phenomena may be alternated if the lines are long enough in the lossless system. The spacial field distributions of the $E_x(x,y,t)$ at$z$=50Δz. are also observed at 300, 500 and 700 time steps shown in Figure 5.7-5.9.

Figure 5.2 *Ex(y,z,t)* at 200 time steps

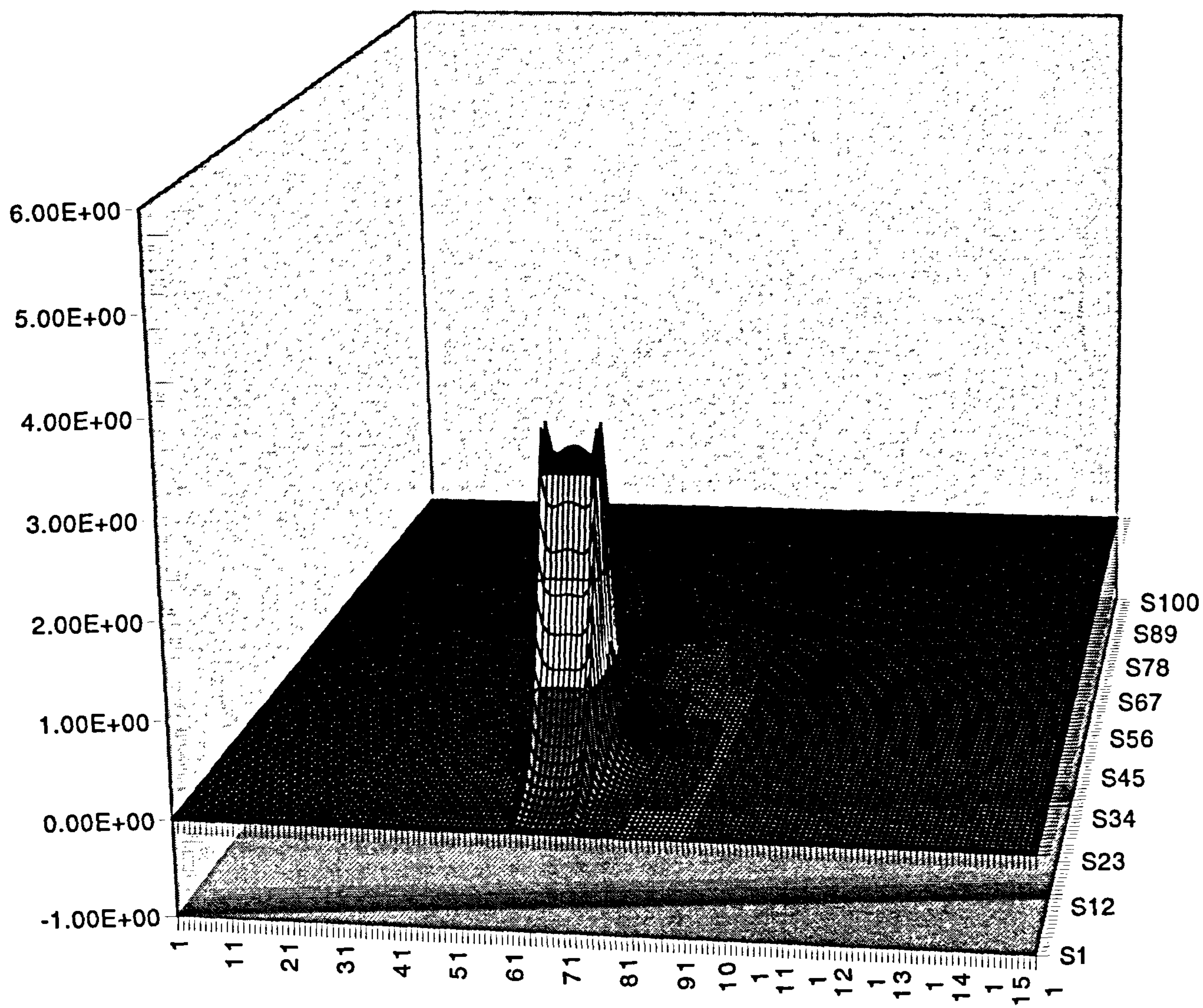

Figure 5.3 *Ex(y,z,t)* at 400 time steps

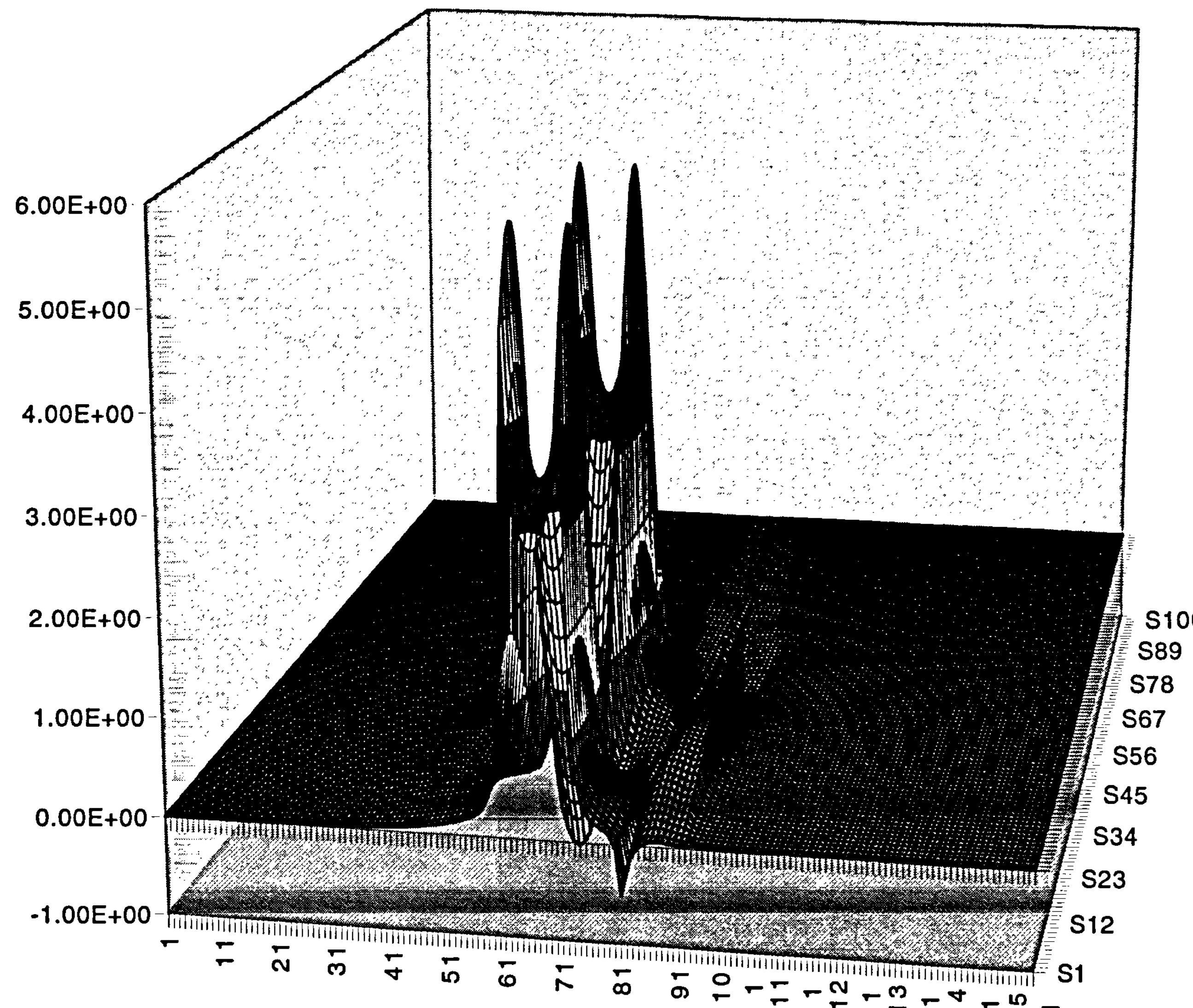

Figure 5.4 *Ex(y,z,t)* **at 600 time steps**

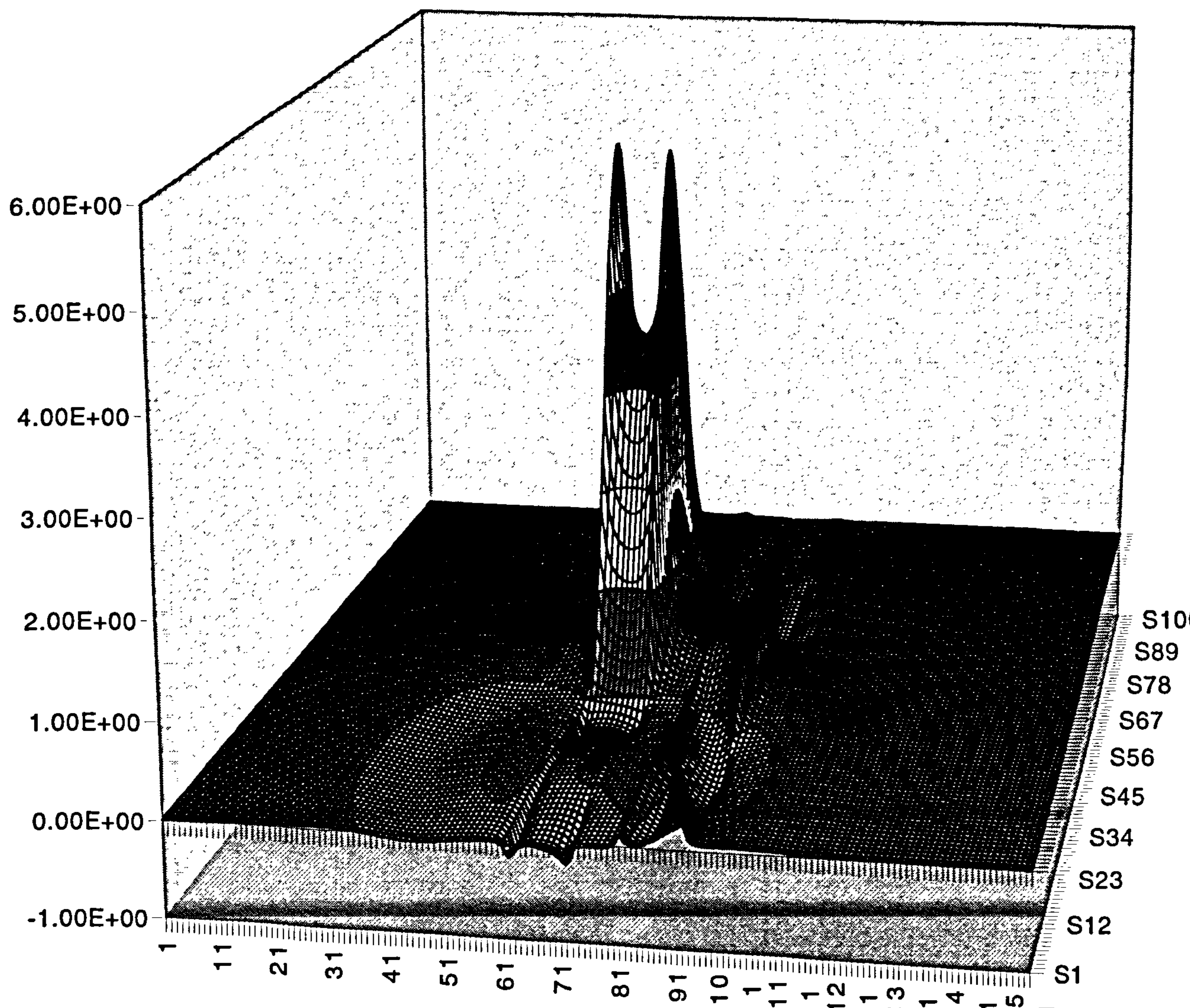

Figure 5.5 *Ex(x,z,t)* at 800 time steps

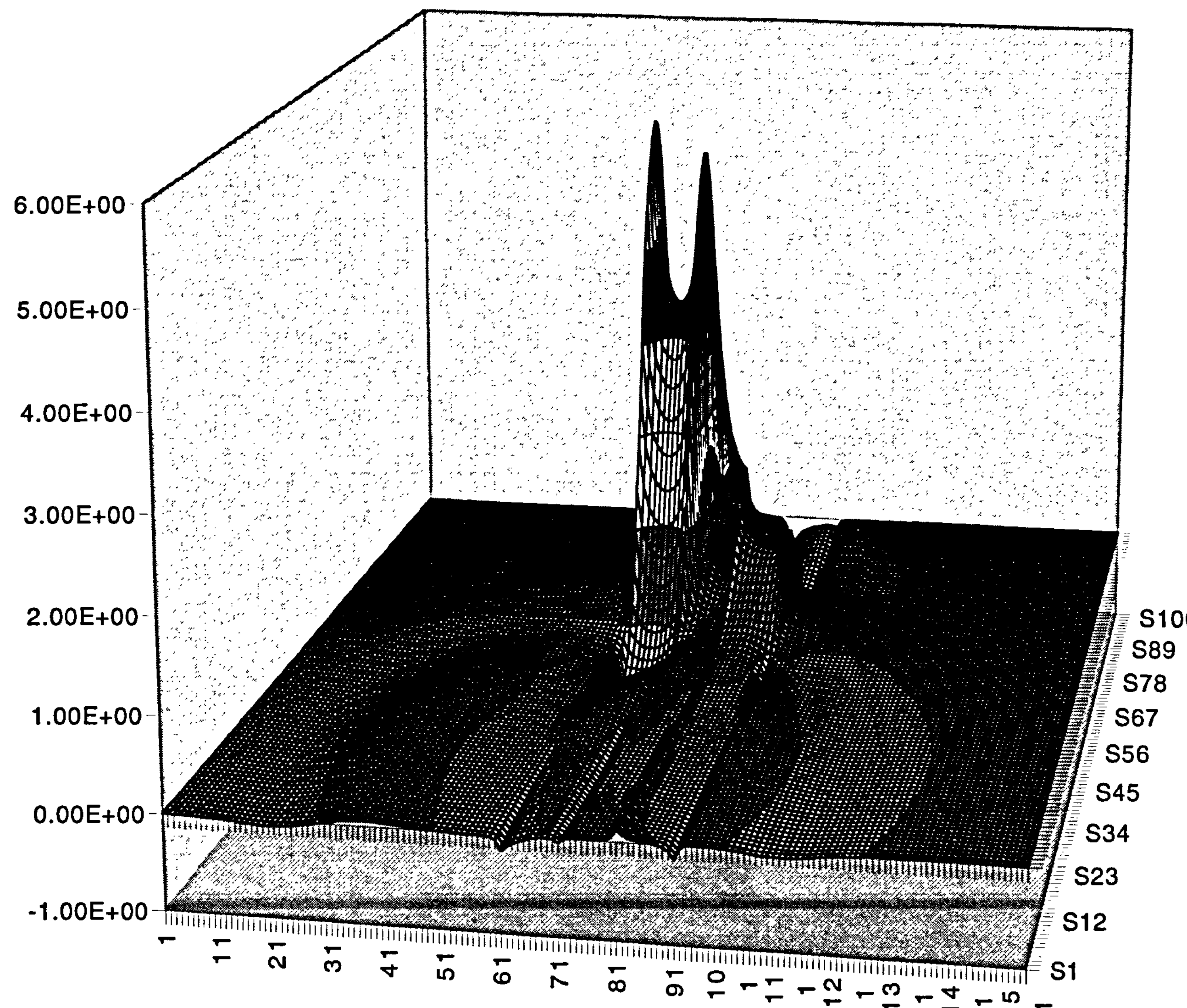

Figure 5.6 *Ex(x,z,t)* at 1000 time steps

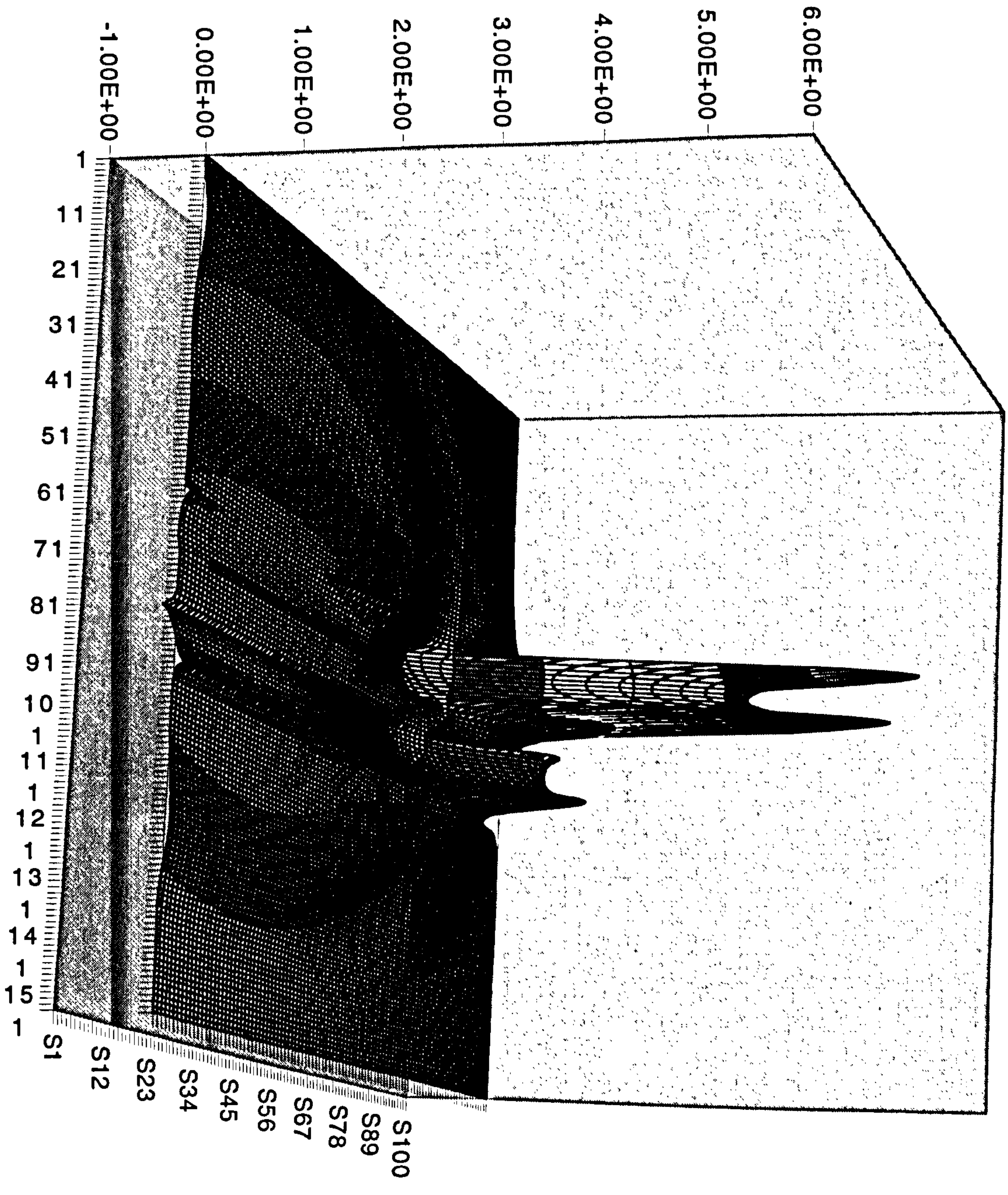

Figure 5.7 *Ex(x,y,t)* at 300 time steps

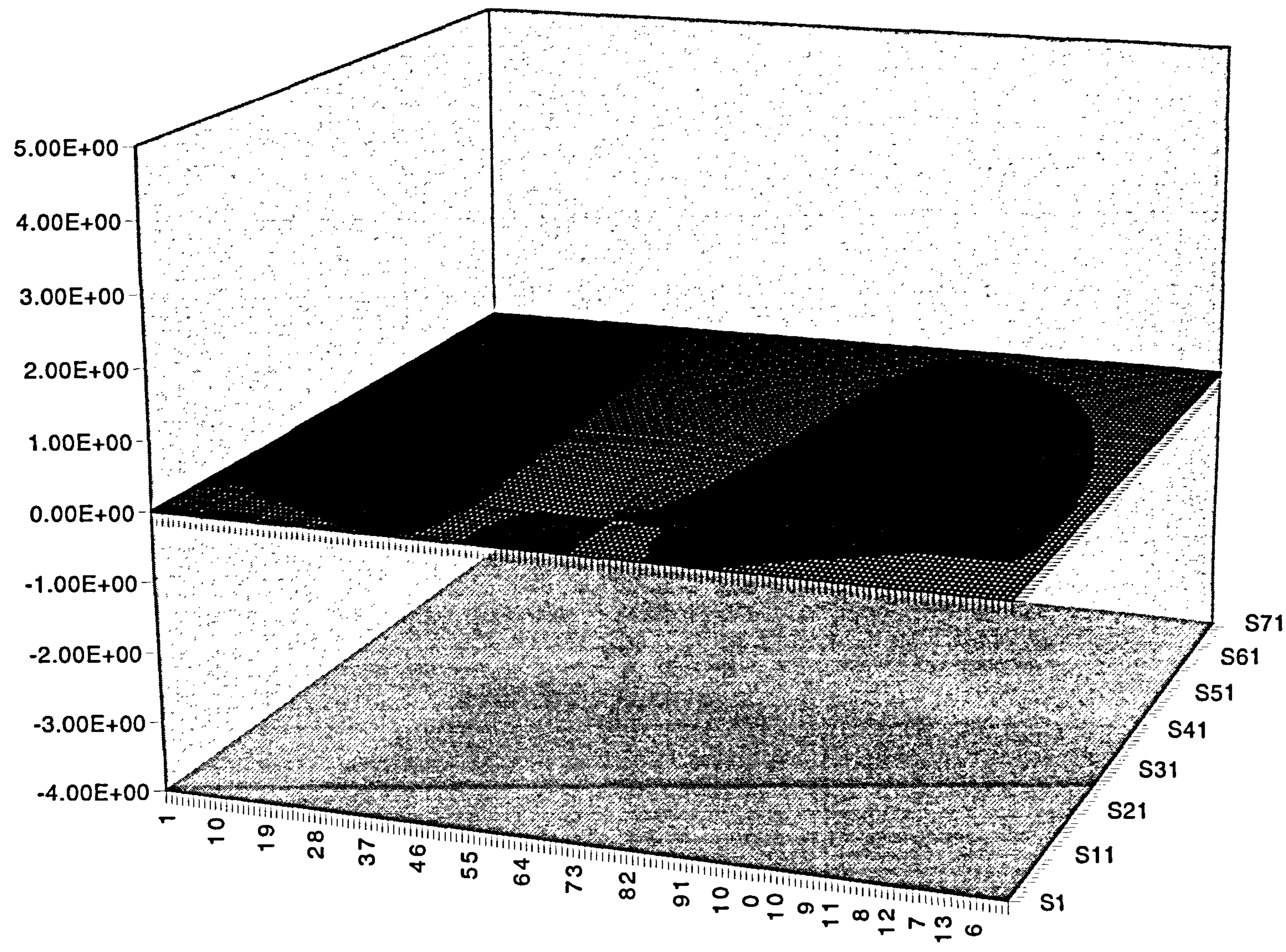

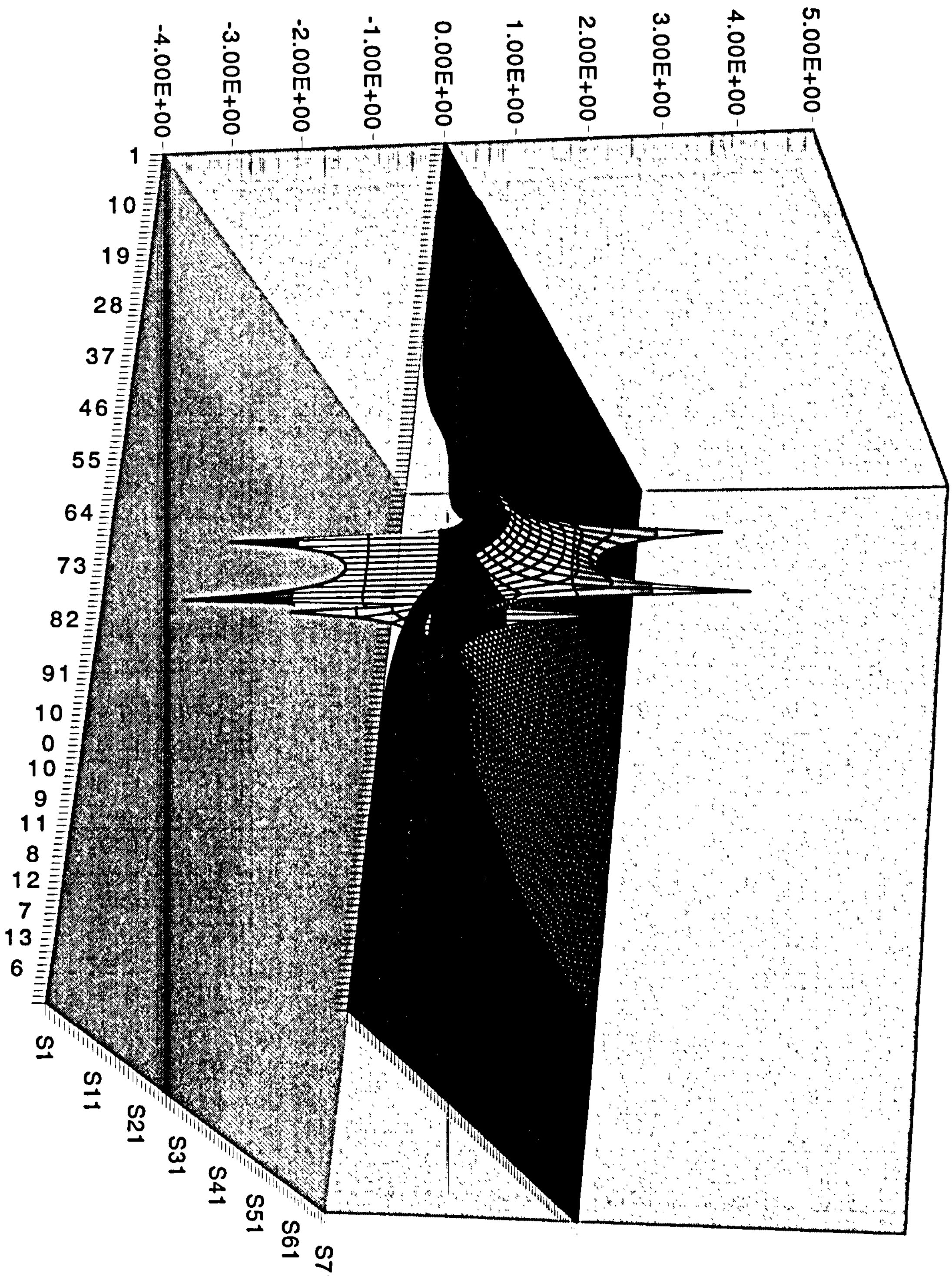

Figure 5.8 *Ex(x,y,t)* **at 500 time steps**

Figure 5.9 *Ex(x,y,t)* at 700 time steps

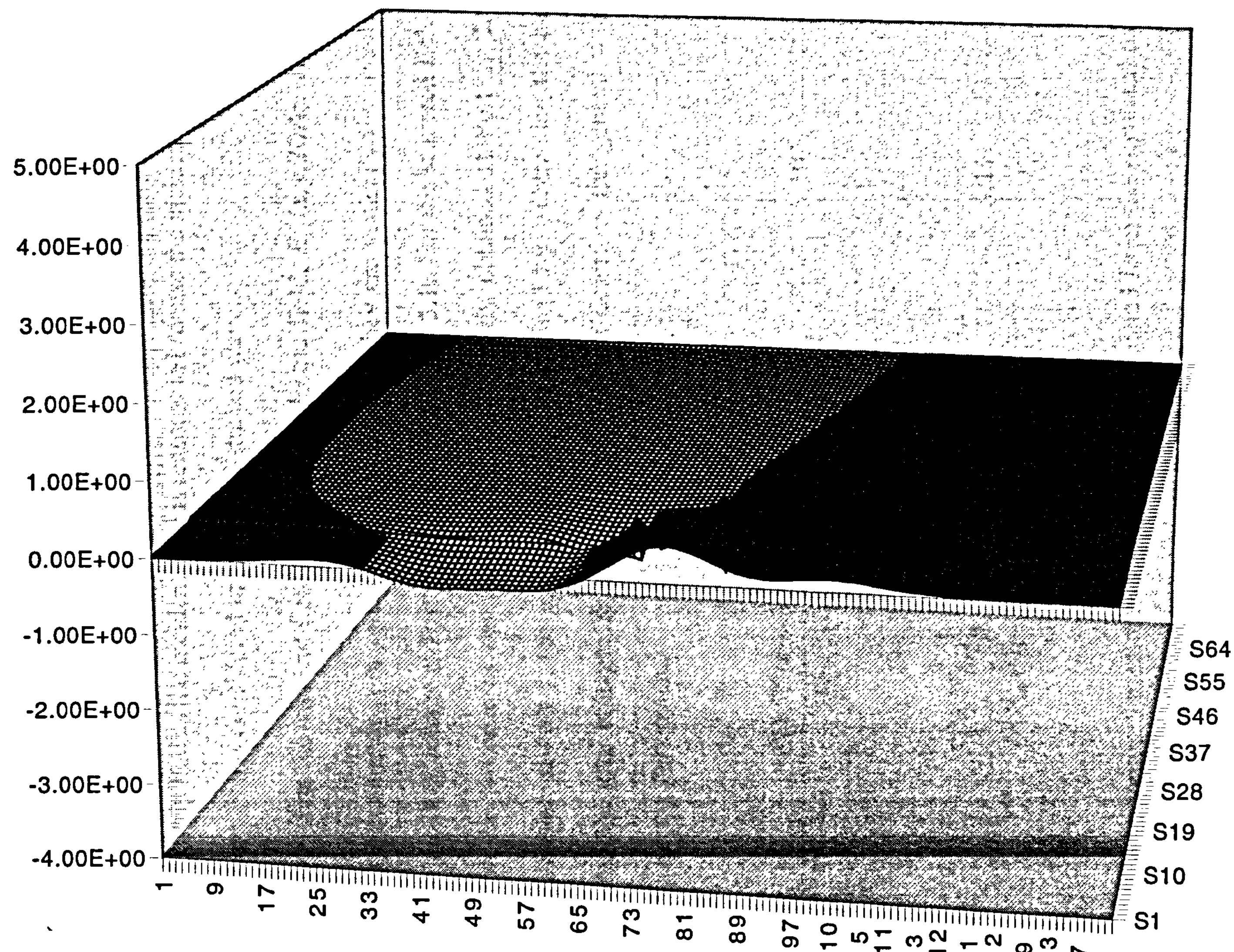

V.2.2 Scattering parameters of coupled microstrip line

Scattering problems usually involve a known incident field and unknown scattered fields. In this study, the field of a single microstrip line is isolated, numerically simulated and treated as an incident field. The unknown field is the scattered field induced by the presence of a second conductor. Therefore, the assumption of treating the field of a single microstrip line as the incident field is reasonable because the incident wave is the reference wave which is considered to be an undisturbed wave.

For the incident field, the vertical electric field, $E_{x1}(x,y,70\Delta z,\ t)$ underneath the single conductor is recorded as time marches. They are vertically integrated to calculate the incident voltage at Port 1 as specified in Figure 5.1. For the scattered fields, the fields with the presence of the second line, can be easily obtained at Port 1, 2, 3 and 4. However, at Port 1, the reflected voltage is obtained by subtracting the incident wave from the total voltage. The following expression describes the general situation of the scattering parameters.

$$S_{i,j}(\omega)\Big|_{i=j} = \frac{F\left\{V_i^{total}(t) - V_{inc}(t)\right\}}{F\left\{V_{inc}(t)\right\}} \qquad 5.10$$

$$S_{i,j}(\omega)\Big|_{i\neq j} = \frac{F\left\{V_j^{total}(t)\right\}}{F\left\{V_{inc}(t)\right\}} \qquad 5.11$$

Two important S parameters S_{11} and S_{14} are calculated from the simulated data and plotted as a function of frequency shown in Figure 5.10.

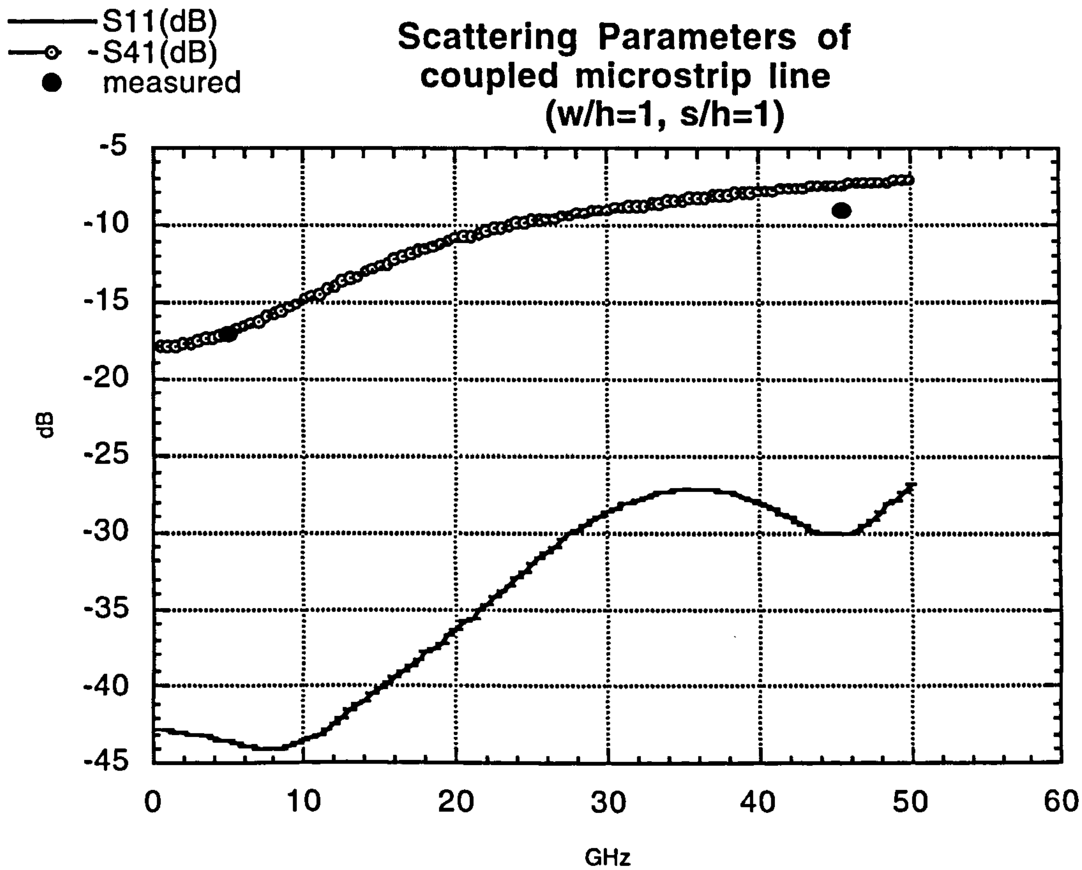

Figure 5.10 Simulated and Measured Scattering Parameters as a function of frequency

Based on the premise that scaling results of the coupled lines can be predicted by the dimensional analysis, experimental measurements are carried out on a coupled lines with dimensions different than the simulated dimensions. The experimental circuit line width w, line separation, s and substrate height, h are chosen so that it has the same s/h and w/h ratios and the same dielectric constant as simulated in the FDTD analysis. The dielectric constant of the substrate is identical for the two cases.

As mentioned in Section V.2.1, the circuit dimension of the computational domain is on the order of $3.5mm$ x $7.5mm$ x $1.25mm$. The conductor is treated as PEC with zero thickness. The width of the conductor and spacing between two conductors are selected based on dimensional analysis. The total length of the conductor line is $1.25mm$ which is equivalent to $25\Delta z$. The operating frequency of interest is from dc to 50GHz. Although the numerical results are also evaluated at higher frequencies, we only examined the results at the lower frequencies because of the potential numerical dispersion at the higher frequencies. The circuits were also simulated on the commercial circuit simulations software, such as Libra and Microwave Harmonica.

The experimental circuits were fabricated on Duroid substrate with ε_r=10 and thickness of $20mil$. The length of the conductor lines of the experimental circuit was 50 mm which was forty times longer than the length of the simulated structure. The widths and the separation distance are chosen to have the same s/h and w/h ratios as in the simulations.

Scattering parameters were measured using an HP8510 and compared to the numerical results as shown in Figure 5.10. Although two measured data points are compared to the simulated data, they show very good agreement between the FDTD and experimental results.

One thing of interest to point out is that as pointed out in the dimensional analysis, the coupled scattering parameter, S_{14} can be described as a function of the product of conductor length and frequency divided by the speed of light, which is

$S_{14} = f(\frac{frequency \cdot length}{c})$, not as a function of frequency alone. This relationship gives a π-term which holds true as long as the other system parameters are assumed to be remained same. For example, as shown in Figure 5.10 the resonance occurred for the both simulated and measured circuits at the product of conductor length and frequency divided by the speed of light about 0.0375 and 0.1875.

V.2.3 Even and Odd modes [24]

The coupled microstrip lines involve three conductors (two signal lines and one ground plane) in the system. Therefore, two fundamental modes of propagation are assumed for the solution. Since two conductor lines are surrounded by inhomogeneous dielectric materials, the fundamental mode is not pure TEM. However, two quasi-TEM modes, even and odd modes, are assumed to be fundamental modes of propagation and consequently the overall solution is the linear combination of these two modes. Figure 5.11 shows the simple schematic representation of the even and odd modes..

The electric field of even mode is symmetrical to the center line and its horizontal component vanishes at this center line. For the odd mode, however, one conductor line holds a positive potential whereas the other conductor holds a negative potential. And thus, an odd symmetric electromagnetic field exists relative to the center line which hold a zero potential, same as the ground plane.

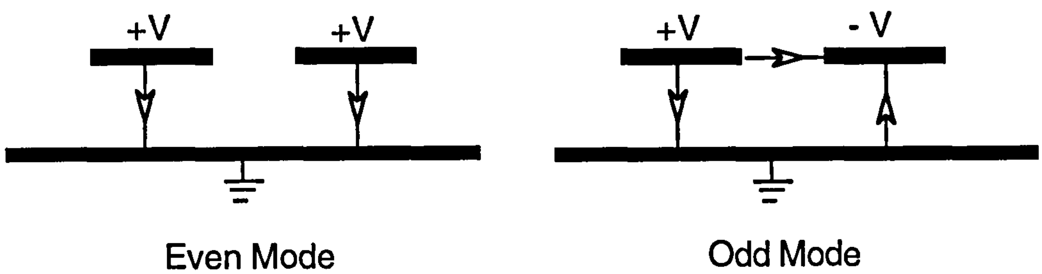

Figure 5.11 Simple representation of the Even and odd modes.

Because of this quite different electromagnetic field distributions, the effective dielectric constant and characteristic impedance of the odd mode substantially different from those of the even mode. As shown in Figure 5.11 the high field region of the even mode is mainly in the substrate, whereas a significant portion of the high field region of the odd mode is in the air. Therefore, one would expect the effective dielectric constant is larger for the even mode than for the odd mode. This is verified by the numerical results which will be shown later. For the characteristic impedance, it is hard to visualize, but we can qualitatively discuss using the following expression describing the characteristic impedance as a function of L and C

$$Z_o = \sqrt{\frac{L}{C}} \qquad 5.12$$

Compared to even mode the odd mode has a larger C due to the coupled electric field and the smaller L due to the mutual annihilation of the magnetic field from the apposite directional current. Therefore, the characteristic impedance of odd mode is always less than the characteristic impedance of even mode.

Figure 5.12 shows the characteristic impedance of even and odd modes as a function of frequency. The results were obtained from a full wave analysis using FDTD. The simulation was performed on coupled microstrip lines as shown in Figure 5.1. The two conductor lines lay on the top of a substrate with a thickness, h=500um and a dielectric constant of 10. The ratio of conductor width, w and h, is 1, the ratio of the spacing, s and h is also 1. The conductors were treated as perfect electric conductor(PEC) with zero thickness.

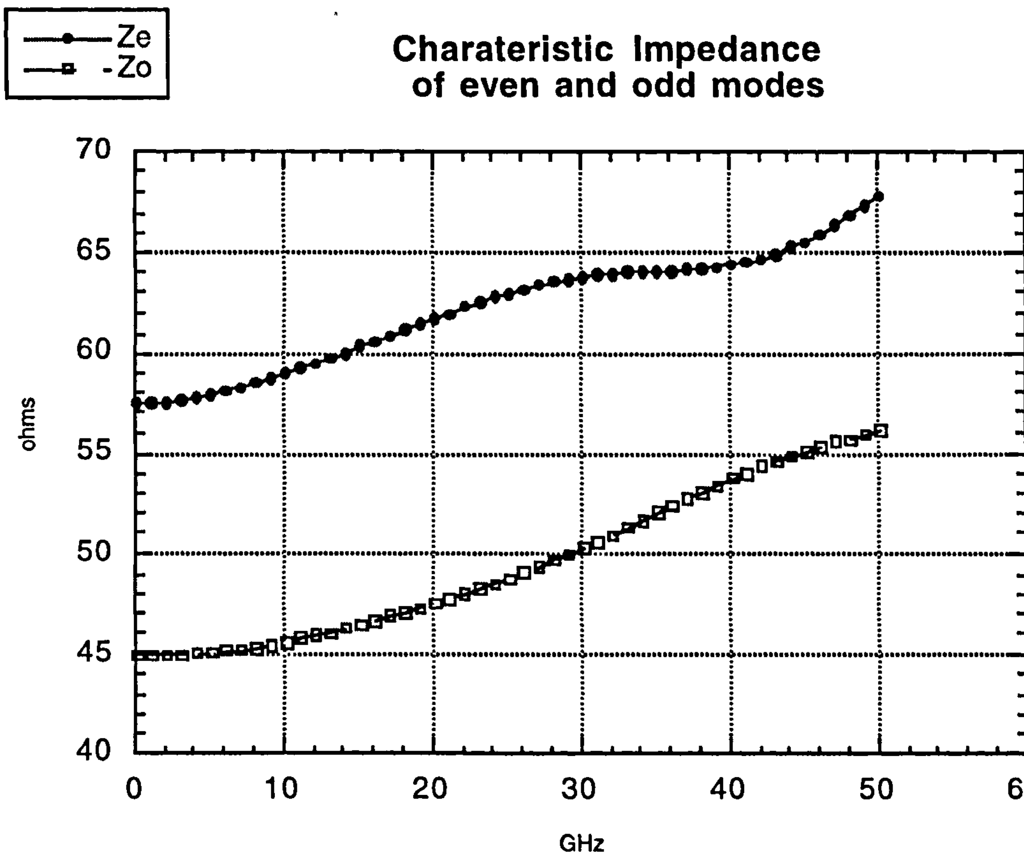

Figure 5.12 Characteristic Impedance of even and odd mode as a function of frequency

Another important microwave parameter, propagation constant is described by

$$\beta = \omega\sqrt{\mu_0\varepsilon_0}\sqrt{\varepsilon_{eff}} = k_0\sqrt{\varepsilon_{eff}}$$

Figure 5.13 shows the square root of the effective dielectric constant obtained from $\frac{\beta}{k_0} = \sqrt{\varepsilon_{eff}}$, where the propagation constant β is factored out by the free space propagation constant, k_o. The corresponding propagation constants obtained from FDTD analysis are shown in Figure 5.14. The propagation constant of even mode tends to be larger than the propagation constant of odd mode because of the coupled electric field which may disturb the guided wave under the substate. Therefore, the discrepancy of propagation constant of two different modes enhances dispersion which already exists in quasi-TEM mode.

As the frequency increases the electric field is more confined to the region between the conductors and the ground plane(Gardiol). As the electric field distribution changes with frequency in the system, it effects the $\sqrt{\varepsilon_{eff}}$ and thus, the propagation constant varies with frequency. As the propagation constant is no longer a linear function of frequency, the phase velocity $\left(v_p = \frac{\omega}{\beta}\right)$ deviates from group velocity $\left(v_g = \frac{d\omega}{d\beta}\right)$.

Therefore, different operating frequency components of an information carrying signal propagates with different velocities and consequently the signal is distorted. As shown in Figure 5.15, the phase velocity of this particular coupled microstrip line changes with frequency around 40GHz.

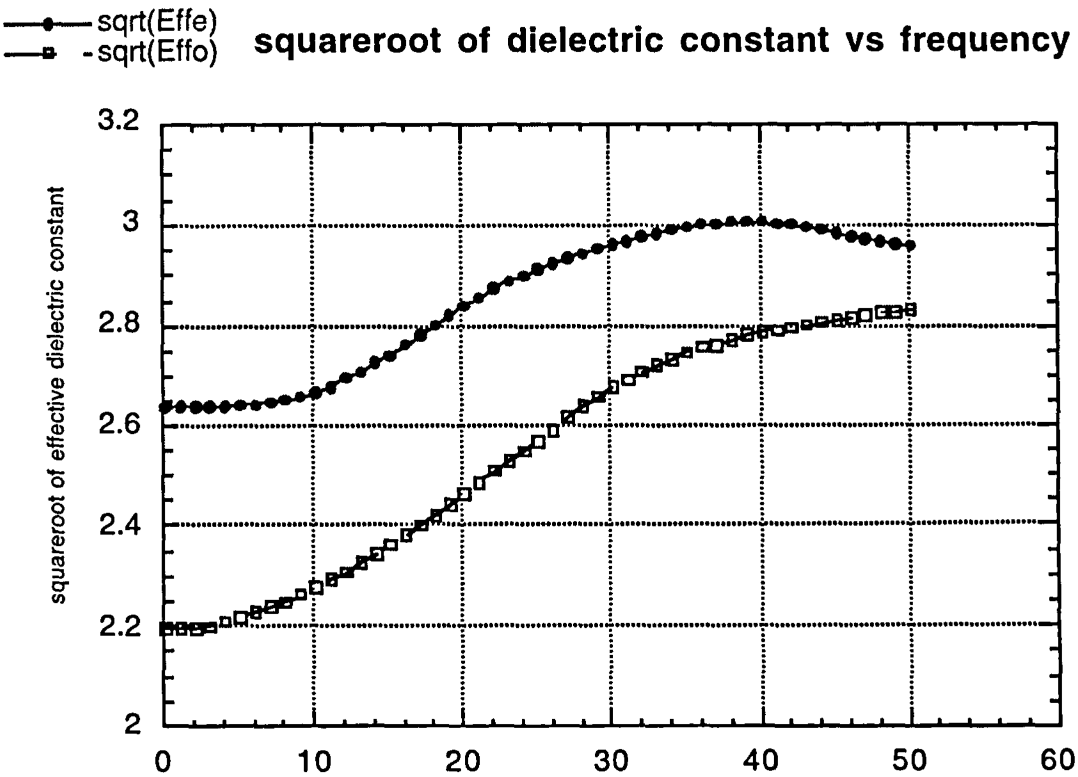

Figure 5.13 Square root of dielectric constant as a function of frequency

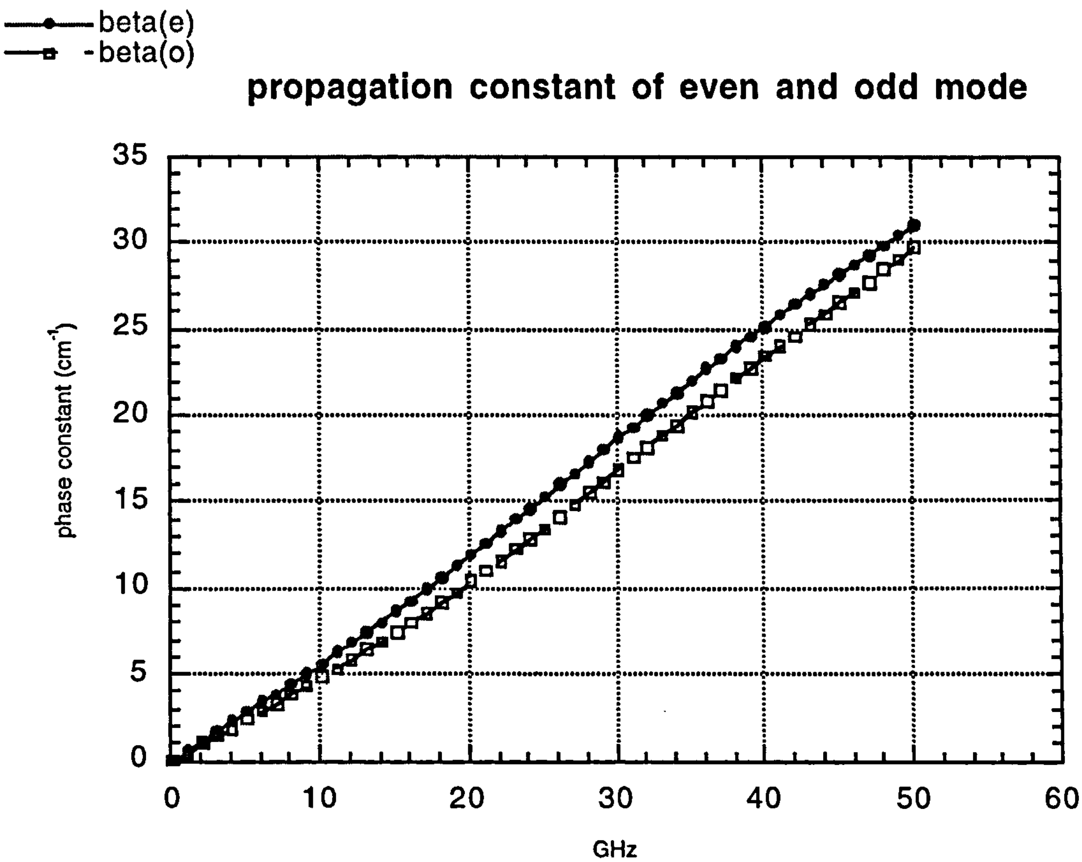

Figure 5.14 Propagation constnat vs. Frequency

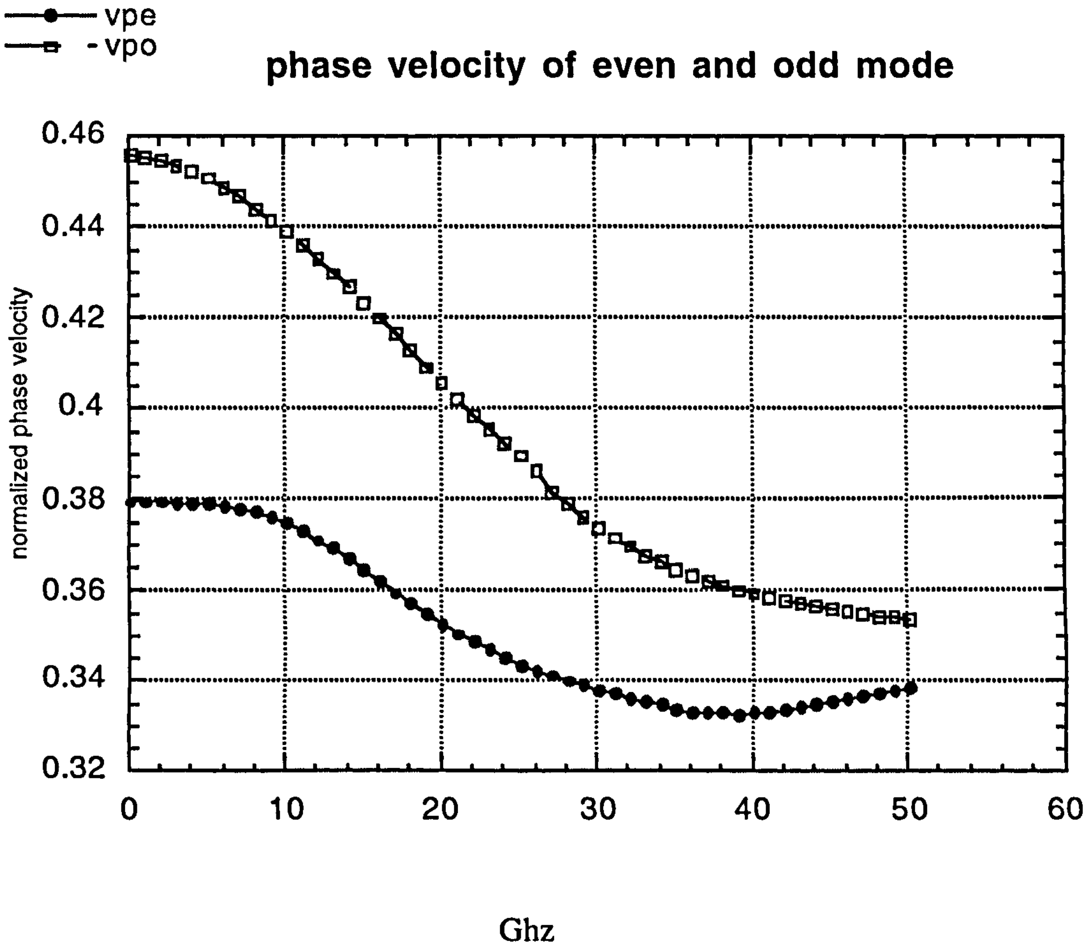

Figure 5.15 Phase velocity of even and odd mode vs frequency

V. 2.4 Coupling Coefficients

The coupling coefficient is a very useful parameter commonly used to design microwave filters and directional couplers. The coupling coefficient is driven from the transmission line theory (pozar). As mentioned previously, the solution of the coupled microstrip lines is a linear combination of even and odd modes. Therefore, the input impedance at *Port 1* can also be described in terms of the linear combination of even and odd voltages and currents.

The configuration of the coupled lines shown in Figure 5.1 was also used for the determination of coupling coefficient. Figure 5.16 shows the schematic of the experimental circuit. As shown in Figure 5.16, if Port 4 happens to be desired coupled port, the coupling coefficient is given by $C_{coefficient} = -10\log\left|\frac{p_4}{p_1}\right| dB$ (ref Inder Bahl) or $C = \frac{Z_c^e - Z_c^o}{Z_c^e + Z_c^o}$ assuming $Z_c = \sqrt{Z_c^e Z_c^o}$. In this study the latter definition was used to calculate the coupling coefficients.

Figure 5.17 depicts coupling coefficient as a function of conductor line width and frequency. As predicted, the narrower conductor lines tend to show larger coupling coefficients probably due to the more edge effect than the wider conductor lines. Three structures are compared with a variation only in the width. The structure 111(1) which is composed of one third line width of the structure 131(3) shows substantially high coupling coefficients over 131(3). This might be attributed to the higher charge density due to the edge being close together. However, the wider lines show some resonance behavior at the higher frequency maybe due to the higher order modes that appears at high fequencies(fdtdref6). It is fairly evident that the narrower spacing between two conductor lines demonstrates higher coupling as shown in Figure 5.18. For Figure 5.19

dimensional analysis was implemented to the FDTD analysis. It was found that although the π-terms are established for the FDTD analysis, the number of spatial step, Δ for the different structure has to be satisfied to complete the meaningful analysis. As shown in Figure 5.19, the thickness, h of the structure 112(7) is 500um whereas the h of 213(8) is 100um. If the same spatial step, say Δ=50um is used for the both structures for the FDTD analysis the structure 213(8) will have only two number of grid points whereas 112(7) will have five number of grid points. This does not allow the 213(8) get simulated with equal accuracy. Therefore, the number of grid points have to be matched as it simulates different structures. Figure 5.19 shows a good agreement between two structures based on dimensional analysis. However, Figure 5.20 shows the better agreement between the two scaled structures because the coupling coefficient is plotted as a function of $\frac{h \cdot f}{c}$, rather than f only, where h,f and c are the thickness of the substrate, frequency and the speed of light, respectively. This is because the term, $\frac{h \cdot f}{c}$ is a π term which is a dimensionless product where as f only is not a dimensionelss product. This also means that to have a true comparison between the two different scaled structures the comparison has to be made in the dimensionless product.

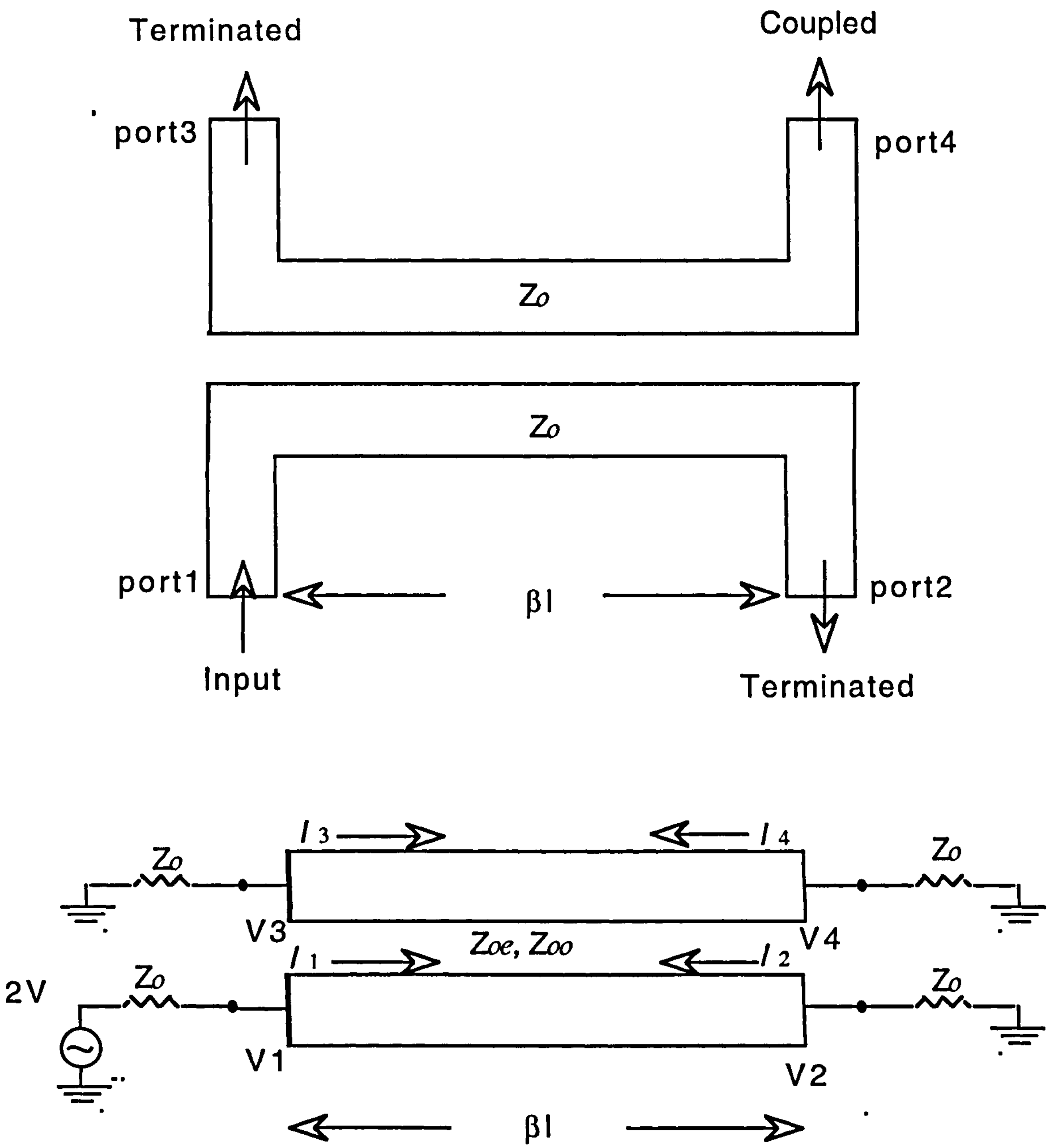

Figure 5.16 Geometry, port destination and the schematic circuit

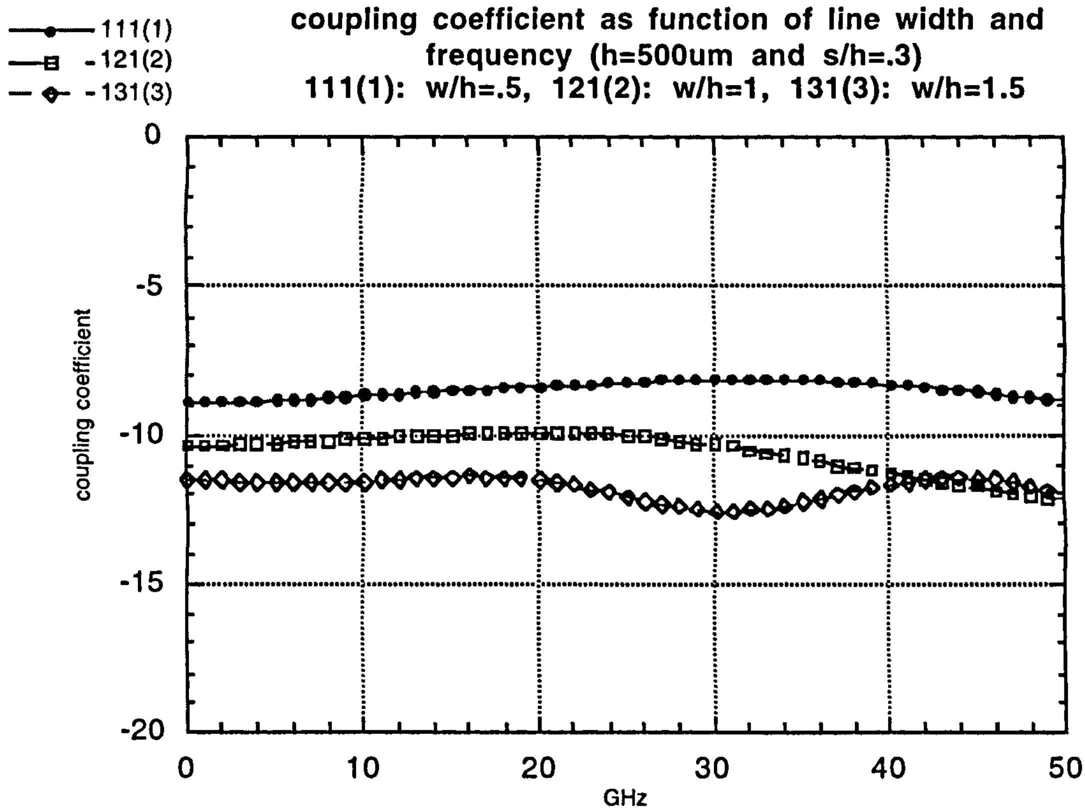

Figure 5.17 Coupling coefficient as function of conductor width and frequency

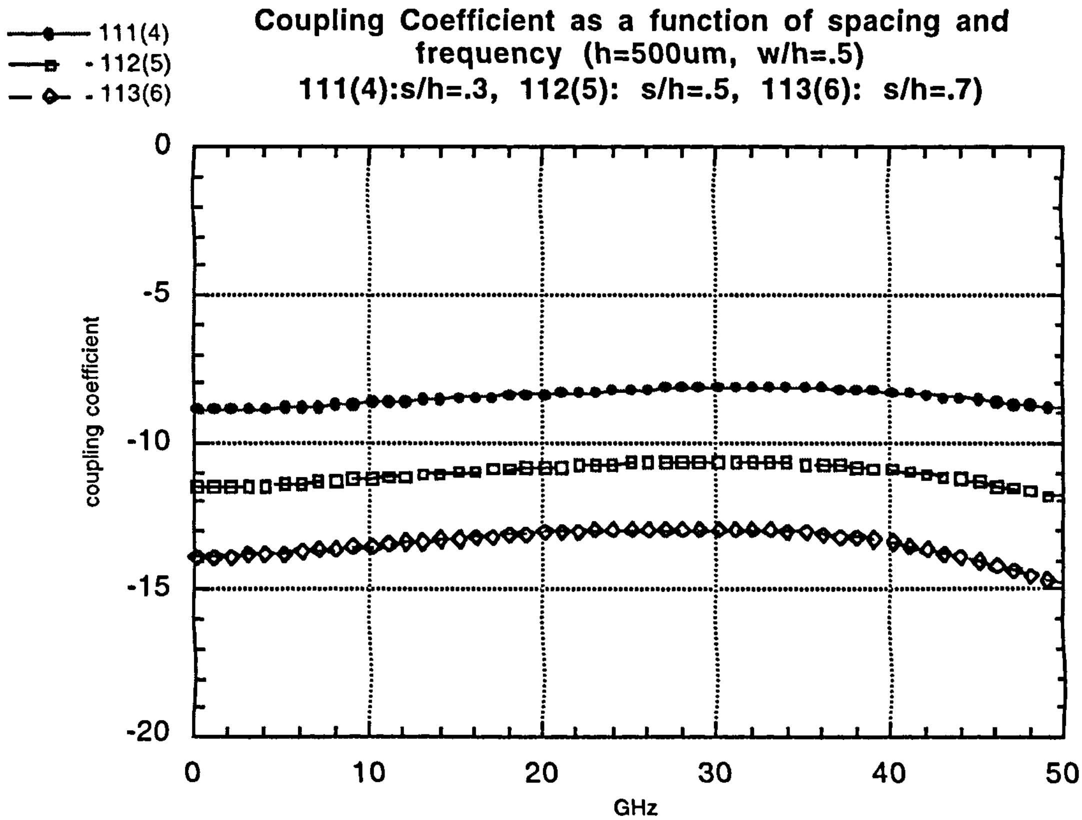

Figure 5.18 Coupling coefficient as function of spacing and frequency

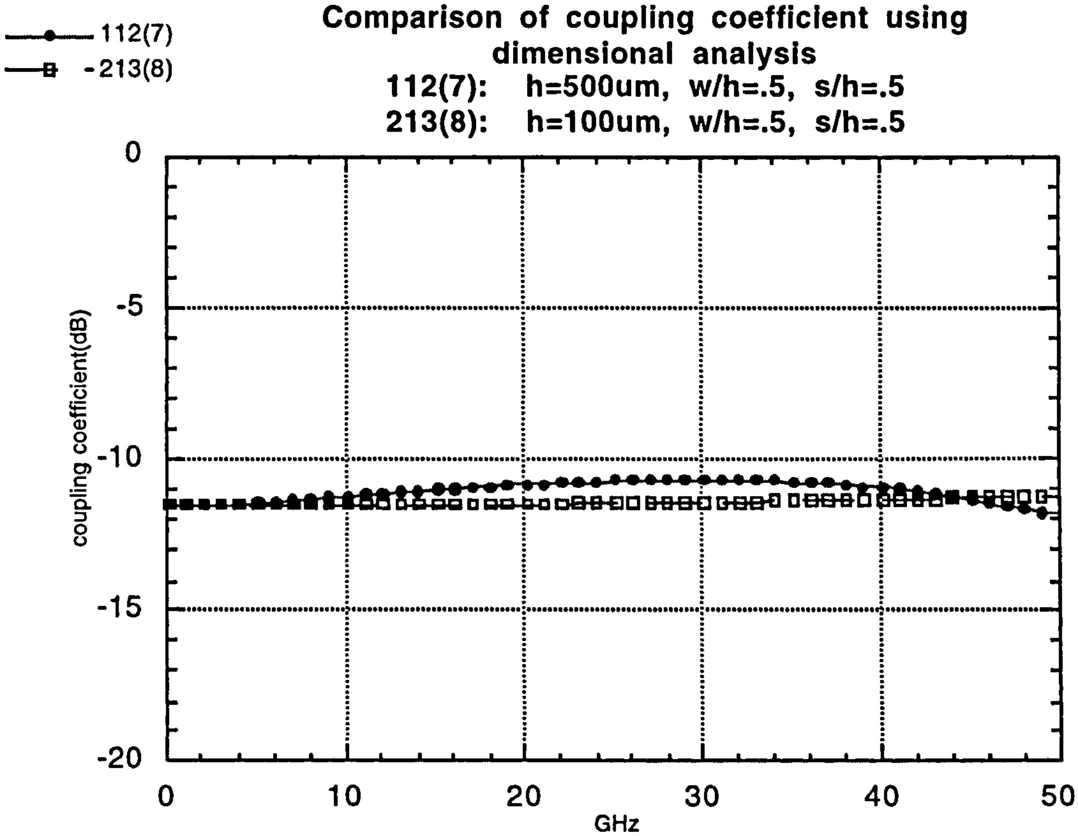

Figure 5.19 Comparison of coupling coefficient as function of frequency using dimensional analysis

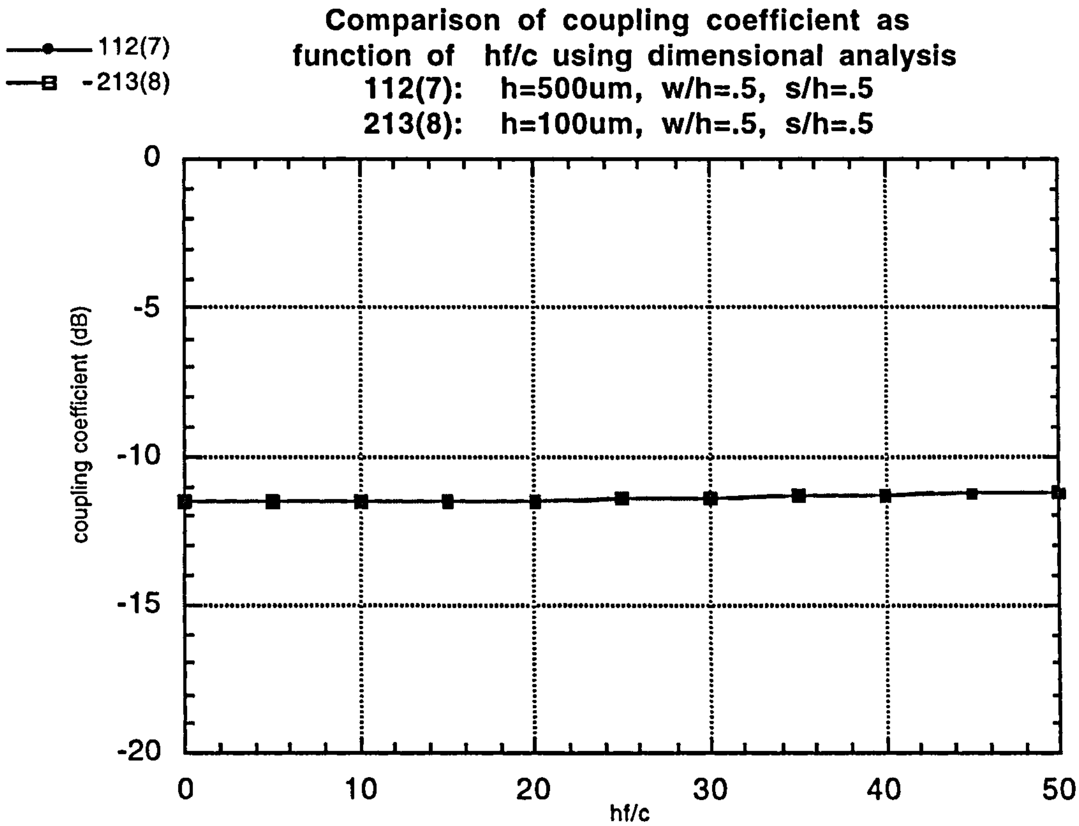

Figure 5.20 Comparison of coupling coefficient as function of hf/c using dimensional analysis

VI.5 Equivalent Circuit Model

To develop the equivalent circuit model, the values of capacitance and inductance are obtained from FDTD results. Capacitance is calculated from $C = \frac{Q}{V}$ where Q is the total charge on the strip conductor and V is the potential difference between the strip conductor and the ground plane. To find the total charge Q, electric flux density is integrated over the surface enclosing the strip conductor as given by Gauss' law: $Q = \oint \vec{D} \cdot d\vec{a} = \oint \varepsilon \vec{E} \cdot d\vec{a}$. The potential difference is obtained by integrating the electric field over the path from the strip conductor to the ground as shown in Equation 5.2.

Inductance is obtained from $L = \frac{\Psi}{I}$, where Ψ is the magnetic flux linkage and I is the current. These are calculated from $\Psi = \int \vec{B} \cdot d\vec{a}$ and $I = \oint \vec{H} \cdot d\vec{l}$, where $\vec{B}$ is magnetic flux density.

Traditionally, the equivalent circuit model has been developed from the scattering parameters. The scattering parameters typically are fed into the lumped element model shown in Figure 5.21 to find the values for capacitance, inductance, resistance and conductance. However, using FDTD analysis capacitance and inductance values are easily and directly obtained from the electric and magnetic field solutions as described above. In other words, characteristic impedance Z_c and propagation constant β,

$Z_c^e = \frac{1}{Y_c^e} = \sqrt{\frac{L^e}{C^e}}$ and $\beta^e = \omega\sqrt{L^e C^e}$ for even mode, and $Z_c^o = \frac{1}{Y_c^o} = \sqrt{\frac{L^o}{C^o}}$ and $\beta^o = \omega\sqrt{L^o C^o}$ are obtained. With these parameters, ABCD matrix elements can be calculated [8] for the coupled lines suing the following equality:

$$\begin{bmatrix} A & B \\ C & D \end{bmatrix} = \begin{bmatrix} \cos\beta l & jZ_c \sin\beta l \\ jY_c \sin\beta l & \cos\beta l \end{bmatrix} \qquad 5.14$$

The ABCD matrix is then converted to the following scattering matrix:

$$\begin{bmatrix} S_{11} & S_{12} \\ S_{21} & S_{22} \end{bmatrix} = \begin{bmatrix} \dfrac{A+B/Z_c-CZ_c-D}{\Delta} & \dfrac{2(AD-BC)}{\Delta} \\ \dfrac{2}{\Delta} & \dfrac{-A+B/Z_c-CZ_c+D}{\Delta} \end{bmatrix} \qquad 5.15$$

Finally, using the four port network of the coupled lines, the following expressions are used to calculate the scattering matrix elements.

$$S_{11} = \frac{1}{2}S_{11}^e + \frac{1}{2}S_{11}^o \qquad 5.16$$

$$S_{21} = \frac{1}{2}S_{21}^e + \frac{1}{2}S_{21}^o \qquad 5.17$$

$$S_{31} = \frac{1}{2}S_{11}^e - \frac{1}{2}S_{11}^o \qquad 5.18$$

$$S_{41} = \frac{1}{2}S_{21}^e - \frac{1}{2}S_{21}^o \qquad 5.19$$

Since FDTD analysis uses the full vector analysis, the scattering parameters calculated using the capacitance and inductance values from the FDTD results will be more reliable and straight forward to be implemented in the microwave circuit design.

The equivalent circuit parameters shown in Figure 5.21 can be extracted from the even and odd mode simulations of FDTD results of coupled microstrip lines.

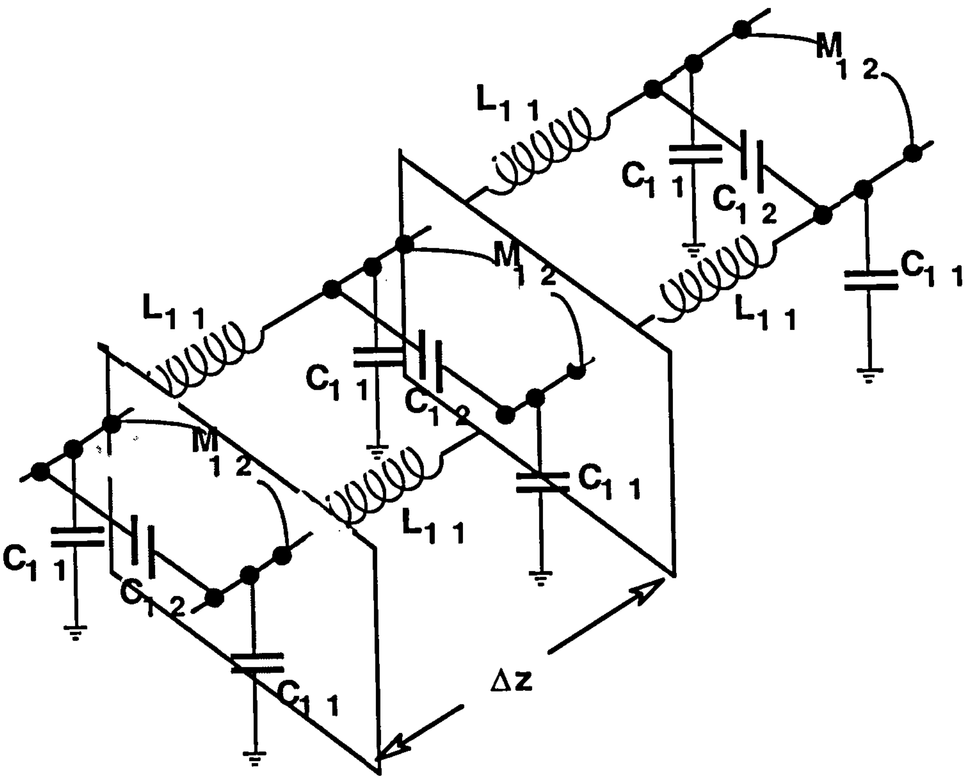

Figure 5.21 Lumped element model of the coupled microstrip line

CAHAPTER VI. Discussion and Future Work

In this thesis, with the 3D MMIC elements development in mind, two rigorous design approaches have been attempted. First, dimensional analysis, a non-conventional methodology has been performed in scaled single microstrip lines to obtain the mathematical design expressions as a function of dimensionless products, π-terms. The design expressions have been driven for characteristic impedance and effective dielectric constant for the low and high frequency approximations. The analysis of mechanism for conductor and dielectric loss have been also discussed. However, dimensional analysis is limited to its inherent capability. Since it does not generate its own algebraic analytical solution of the governing equations, it is always required to be relied on other solutions to come up with its own mathematical design expressions.

To enhance the design capability of innovative 3D MMIC elements and to complement dimensional analysis formalism, the finite difference time-domain (FDTD) have been looked into as a full wave field solver which is required to simulate the denser discontinuities of the system. A simple coupled microstrip lines is used to demonstrate the capability of FDTD.

The FDTD has been used to perform time-domain simulations of pulse propagation in scaled coupled microstrip lines. In addition to the time-marching results, frequency-dependent characteristic impedance, effective dielectric constant and phase velocity have been calculated by Fourier transform of the time-domain results. Some results have been verified by comparison with measured data. Most importantly, based on the premise that scaling results can be predicted by the dimensional analysis, experimental measurements are carried out on a coupled lines with dimensions different than simulated ones. Using

FDTD results, an unique approach for developing lumped element models have been also discussed.

This unique approach in conjunction with dimensional analysis can enhance design capability to simulate microwave structures such as coupled strip lines as shown in Figure 6.1 to 6.3. The coupled strip line shown in Figure 6.1, broad strip line shown in Figure 6.2 and general case of strip line shown in Figure 6.3 are basic transmission line structures which can be implemented to 3D MMIC element development. Ultimately it is required to develop the vertical interconnect shown in Figure 6.4 for the further development. Considerable work has already been performed on the coupled structures [25,26,27,29,30]. However, the approach developed in this thesis is unique and can substantially contribute to the 3D MMIC development. The technique is applicable to all possible circuit configurations that can be used in 3D MMIC.

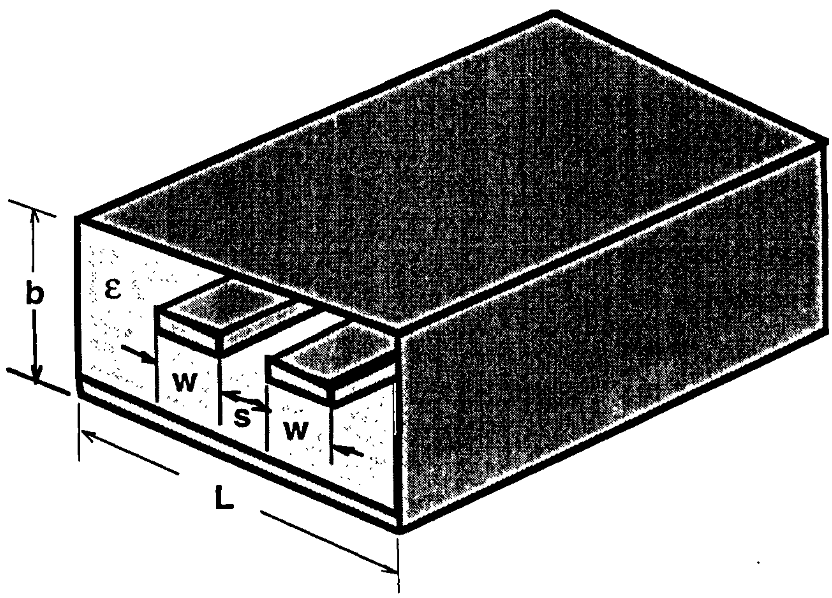

Figure 6.1 Coupled Strip Line

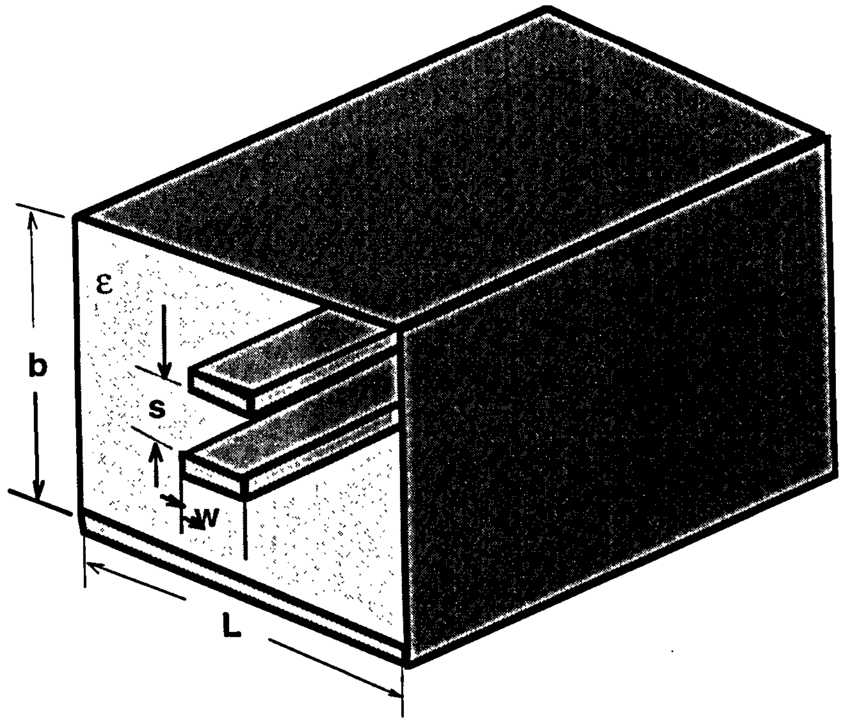

Figure 6.2 Broad Strip Lines

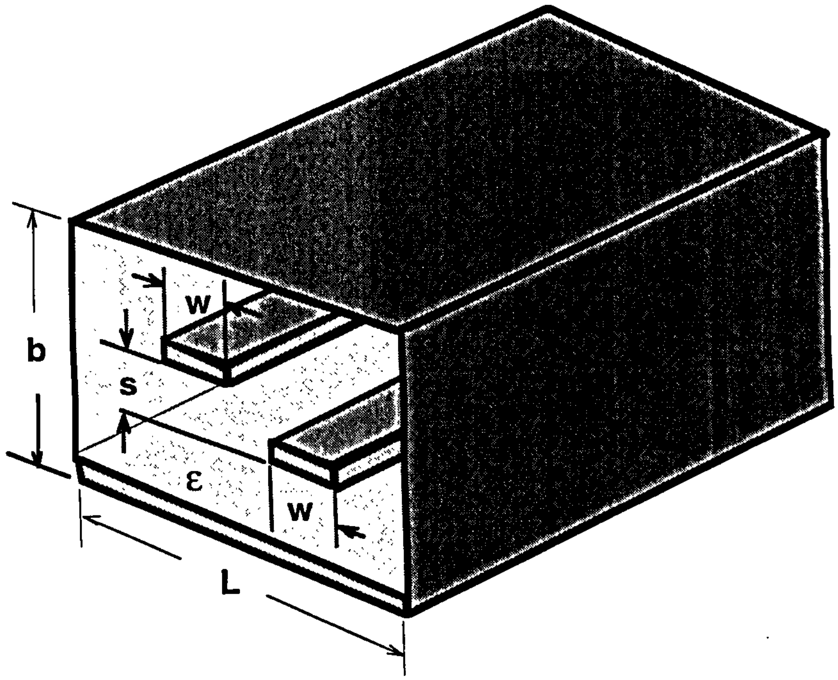

Figure 6.3 General Case of the Coupled Strip Lines

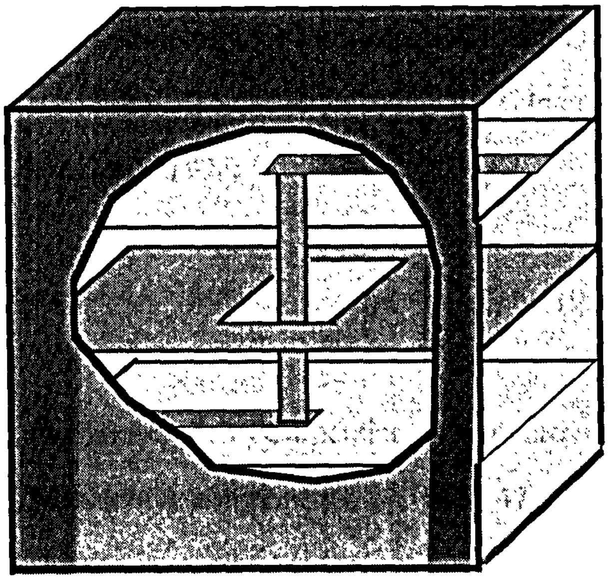

Figure 6.4 Vertical 3D interconnect

REFERENCES

1. R.Hess, "MMICs for Commercial Applications The Low-Cost High Volume Production Techniques," Proceedings IEEE Microwave and mm-wave Monolithic Circuits Symposium, June, 1996.

2. Tokumitsu, K. Nishikawa, K Kamogawa, I. Toyoda and M. Aikawa, " Three-Dimensional MMIC Technology for Multifunction Integration and its Possible Application to Masterslice MMIC," Proceedings IEEE International Microwave Symposium Digest, June, 1996.

3. Gardiol, "Microstrip Circuits," John-Wiley and Sons, Inc., 1994.

4. Smith, Bradford L. and Michel-Henri Carpentier, "The microwave Engineering Handbook," vol.1, Microwave components, pp. 141-147, New York , Van Nostrand Reinhold, 1992.

5. C. Gupta, R. Garg and I. Bahl, "Microstrip Lines and Slotlines," Artech House, Inc., 1979.

6. Gonzalez, "Microwave Transistor Amplifiers Analysis and Design," Prentice- Hall, Inc., 1984.

7. Edwards, T.C and Owens, R.P "2-18 Ghz dispersion measurements on 10-ohms microstrip line on saphire" IEEE Trans. MTT-24, No.8, pp.505-Aug 1976.

8. Pozar, "Microwave Engineering," Addison-Wesley Publishing Company Inc., 1990.

9. A. Stratton, "Electromagnetic Theory," McGraw-Hill, Inc., 1941.

10. P.W Bridgman, "Dimensional Analysis," New Haven: Yale University Press,

11. H.L Langhaar, "Dimensional Analysis and Theory and Models," Huntington, New York: Robert E. Krieger Publishing Company, 1980.

12. Bahl and P. Bhartia, "Microwave Solid State Circuit Design," John-Wiley and Sons, Inc., 1988.

13. W. H. Middendorf, "Design of Devices and Systems," New York: Marcel Dekker, Inc., 1990.

14. B. S. Massey, "Measures in Science and Engineering," New York: John Wiley and Sons, Inc., 1986.

15. Allen Taflove, "Computational Electrodynamics,"Atech House,Inc., 1995

16. Zhiqiang Bi, K. Wu, C. Wu and J. Litva, " A Dispersive Boundary Condition for Microstrip Component Analysis Using The FD-TD Method," *IEEE Trans. Microwave Theory Tech.*,vol. 40, No. 4, pp. 774-777, April 1992.

17. David M. Sheen, S. M. Ali, M. D. Abouzahra and J. A. Kong, "Application of the Three-Dimensional Finite-Difference Time-Domain Method to the Analysis of Planar Microstrip Circuits," *IEEE Trans. Microwave Theory Tech.*,vol. 38, No. 7,

July 1990.

18. Yee, K. S., "Numerical solution of initial boundary value problems involving Maxwell/s equations in isotropic media," IEEE Trans. Antennas and Propagation, vol. 14, pp. 302-307, 1966.

19. Kendall E. Atkinson, "An Introduction to Numerical Analysis," John Wiley and Sons, pp. 147-154, 1988.

20. An Ping Zhao, A. V. Raisanen and S. R. Cvetkovic, "A Fast and Efficient FDTD Algorithm for the Analysis of Planar Microstrip Discontinuities by Using a Simple Source Excitation Scheme," *IEEE Microwave and Guided Waver Letters*. vol. 5. No. 10, pp. 341-343, Oct. 1995.

21. Xiaoleizhang, J. Fang, K. K. Mei and Y. Liu, "Calculations of the Dispersive Characteristics of Microstrips by the Time-Domain Finite Difference Method," *IEEE Trans. Microwave Theory Tech.*,vol. 36, No. 2, Feb 1988.

22. Xiaoleizhang and K. K. Mei, "Time-Domain Finite Difference Approach to the Calculation of the Frequency-Dependent Characteristics of Microstrip Discontinuities," *IEEE Trans. Microwave Theory Tech.*,vol. 36, No. 12, pp. 1775-1788, Dec. 1988.

23. Yuanxun Wang and H. Ling, "Multimode Parameter Extraction for Multiconductor Trasnmission Lines via Single-Pass FDTD and Signal-Processing Techniques," *IEEE Trans. Microwave Theory Tech.*,vol. 46, No. 1, pp. 89-96, Jan. 1998.

24. R. E. Collin, "Foundations for Microwave Engineering," McGraw-Hill Electrical and Computer Engineering Series, McGraw-Hill, Inc., 1992.

25. Kiang, Jean-Fu; Ali, Sami M.; Kong, Jin A.,"Integral Equation Solution To The Guidance And Leakage Properties Of Coupled Dielectric Strip Waveguides," Ieee Transactions On Microwave Theory And Techniques, V38 N2 P193-203 Feb 90.

26. Shelton, J. P., Jr. "Impedances of offset parallel- coupled strip transmission lines," IEEE Transactions Microwave Theory And Techniques, Vol. Mtt-14, P. 7-15. Jan.1966.

27. Yuan, Naichang; He, Jianguo; Yao, Demiao; Dai, Qin; Lin, Weigan, "Analysis of some coplanar transmission lines: coplanar coupled lines, coplanar coupled striplines, and coplanar coupled lines with rectangular microshield," Microwave and Optical Technology Letters v 9, No.2, p85-87, Jun 5 1995.

28. Tsitsos, Stelios; Gibson, Andrew A.P., "Higher order modes in coupled striplines: prediction and measurement," IEEE Transactions on Microwave Theory and Techniques vol. 42, No. 11 p 2071-2077, Nov. 1994.

29. BHARTIA, PRAKASH, PRAMANICK and PROTAP, "Computer-aided design models for broadside- coupled striplines and millimeter-wave suspended substrate microstrip lines," IEEE Transactions on Microwave Theory and Techniques, vol. 36, p. 1476-1481. Nov. 1988.

30. Fouladian, Jamshid; Pramanick, Protap, "Generalized analytical equations for strip transmission lines, Microwave Journal vol., 32. No. 11, pp. 165-168, Nov 1989.

31. Schneider, "Microstrip Lines for Microwave Integrated Circuits," The Bell System Technical Journal, vol. 48, pp. 1421-1444, 1969.